THE JOURNAL OF BIOLOGICAL CHEMISTRY Vol. 280, No. 13, Issue of April 1, pp. 12820–12832, 2005
Printed in U.S.A.

Control of Calcium Signal Propagation to the Mitochondria by Inositol 1,4,5-Trisphosphate-binding Proteins*

Received for publication, October 12, 2004, and in revised form, December 27, 2004
Published, JBC Papers in Press, January 11, 2005, DOI 10.1074/jbc.M411591200

Xuena Lin‡§, Péter Várnai§¶, György Csordás‡, András Balla‖, Takeharu Nagai, Atsushi Miyawaki**, Tamás Balla‖, and György Hajnóczky‡ ‡‡**

*From the ‡Department of Pathology, Anatomy & Cell Biology, Thomas Jefferson University, Philadelphia, Pennsylvania 19107, ¶Department of Physiology, Faculty of Medicine, Semmelweis University, P. O. Box 259, H-1444, Budapest, Hungary, ‖Endocrinology and Reproduction Research Branch, NICHD, National Institutes of Health, Bethesda, Maryland 20892, and **Laboratory for Cell Function and Dynamics, Advanced Technology Development Center, Brain Science Institute, RIKEN, 2-1 Hirosawa, Wako-city, Saitama 351-0198, Japan*

Cytosolic Ca^{2+} ($[Ca^{2+}]_c$) signals triggered by many agonists are established through the inositol 1,4,5-trisphosphate (IP_3) messenger pathway. This pathway is believed to use Ca^{2+}-dependent local interactions among IP_3 receptors (IP3R) and other Ca^{2+} channels leading to coordinated Ca^{2+} release from the endoplasmic reticulum throughout the cell and coupling Ca^{2+} entry and mitochondrial Ca^{2+} uptake to Ca^{2+} release. To evaluate the role of IP_3 in the local control mechanisms that support the propagation of $[Ca^{2+}]_c$ waves, store-operated Ca^{2+} entry, and mitochondrial Ca^{2+} uptake, we used two IP_3-binding proteins (IP3BP): 1) the PH domain of the phospholipase C-like protein, p130 (p130PH); and 2) the ligand-binding domain of the human type-I IP3R ($IP_3R_{224-605}$). As expected, p130PH-GFP and GFP-$IP_3R_{224-605}$ behave as effective mobile cytosolic IP_3 buffers. In COS-7 cells, the expression of IP3BPs had no effect on store-operated Ca^{2+} entry. However, the IP_3-linked $[Ca^{2+}]_c$ signal appeared as a regenerative wave and IP3BPs slowed down the wave propagation. Most importantly, IP3BPs largely inhibited the mitochondrial $[Ca^{2+}]$ signal and decreased the relationship between the $[Ca^{2+}]_c$ and mitochondrial $[Ca^{2+}]$ signals, indicating disconnection of the mitochondria from the $[Ca^{2+}]_c$ signal. These data suggest that IP_3 elevations are important to regulate the local interactions among IP3Rs during propagation of $[Ca^{2+}]_c$ waves and that the IP_3-dependent synchronization of Ca^{2+} release events is crucial for the coupling between Ca^{2+} release and mitochondrial Ca^{2+} uptake.

Inositol 1,4,5-trisphosphate (IP_3)[1]-induced Ca^{2+} liberation from intracellular stores results in a $[Ca^{2+}]_c$ signal that controls a wide spectrum of cell functions, including energy metabolism, gene transcription, and cell proliferation. Appropriate exposure of the effectors to Ca^{2+} throughout the cell is supported by several mechanisms that include the propagation of Ca^{2+} release throughout the cell without attenuation, the recruitment of Ca^{2+} entry, and efficient delivery of the $[Ca^{2+}]_c$ signal into organelles such as the nucleus and mitochondria (1).

Spreading of the $[Ca^{2+}]_c$ signal is facilitated by regenerative mechanisms of Ca^{2+} mobilization, which may derive from interactions between adjacent Ca^{2+} release sites. Non-metabolizable IP_3 analogs have been found to evoke $[Ca^{2+}]_c$ oscillations, providing support to the idea that at a constant $[IP_3]$ Ca^{2+} released through IP3Rs is sufficient to trigger regenerative Ca^{2+} release via binding to and activating IP3Rs and ryanodine receptors (RyR) (2). Based on IP_3 microinjection and uncaging studies, the regenerative Ca^{2+} release during $[Ca^{2+}]_c$ waves was also claimed to be largely independent of $[IP_3]$ (3, 4). Along this line, IP3R-mediated $[Ca^{2+}]_c$ waves were observed in the absence of any stimulated IP_3 formation (5). However, released Ca^{2+} may also promote phospholipase C (PLC) activation and, in turn, increase IP_3, providing a potential amplification mechanism for IP3R-mediated Ca^{2+} release waves (6–8). Ca^{2+} may activate the PLC coupled to the agonist receptor to stimulate cleavage of phosphatidylinositol 4,5-bisphosphate (PIP_2) in the plasma membrane. The localization of phospholipase C enzyme isoforms (9, 10) and PIP_2 (11) in intracellular membranes has also been documented. IP_3 formed at the plasma membrane may rapidly diffuse throughout the cytoplasm (12), but the presence of PIP_2 and PLC in the vicinity of the IP3R could also provide for a local IP_3 feedback. Thus, the role of IP_3 fluctuations in Ca^{2+} wave propagation requires further investigation.

Recharging of the ER Ca^{2+} stores during the agonist-induced $[Ca^{2+}]_c$ signal involves Ca^{2+} entry mediated by so-called store-operated Ca^{2+}-entry mechanisms that might be mediated by the canonical transient receptor potential channel family (13). One of the proposed mechanisms for activation of Ca^{2+} entry during Ca^{2+} release is a conformational coupling between IP3Rs and store-operated Ca^{2+} channels (14). Although store-operated Ca^{2+} entry is activated by agents that directly target the ER Ca^{2+} store (15, 16), IP_3 binding to the IP3R has been

* This work was supported by grants from the National Institutes of Health (to G. H.) and by a grant of the Hungarian Science Foundation (OTKA T-034606) (to P. V.). The costs of publication of this article were defrayed in part by the payment of page charges. This article must therefore be hereby marked "*advertisement*" in accordance with 18 U.S.C. Section 1734 solely to indicate this fact.

§ Both authors contributed equally to this work.

‡‡ To whom correspondence should be addressed: Dept. of Pathology, Anatomy and Cell Biology, Rm. 253 JAH, Thomas Jefferson University, Philadelphia, PA 19107. Tel.: 215-503-1427; Fax: 215-923-2218; E-mail: Gyorgy.Hajnoczky@jefferson.edu.

[1] The abbreviations used are: IP_3, inositol 1,4,5-trisphosphate; IP3R, IP_3 receptor; IP3BP, IP_3-binding protein; PH, pleckstrin homology; FRAP, fluorescence recovery after photobleaching; t_{lag}, the lag time needed to reach half of the maximum cytosolic Ca^{2+} response; F_{GFP}, GFP fluorescence; RFP, red fluorescence protein; YFP, yellow fluorescence protein; R_0/R_P, prestimulation ratio *versus* peak response ratio; RyR, ryanodine receptor; PLC, phospholipase C; ER, endoplasmic reticulum; p130, 130-kDa phospholipase C-like protein; $GABA_A$, γ-aminobutyric acid, type A; pericam-mt, pericam targeted to the mitochondria; mito, mitochondrial; BSA, bovine serum albumin; Tg, thapsigargin; ECM, extracellular matrix; EGF, epidermal growth factor; ICM, intracellular medium; $[Ca^{2+}]_m$, mitochondrial matrix $[Ca^{2+}]$; PIP_2, phosphatidylinositol 4,5-bisphosphate.

claimed to have a role in activation of Ca^{2+} entry (17, 18). Nonetheless, the question of whether an increase in $[IP_3]$ is required for the channel activation remains elusive.

IP_3-induced $[Ca^{2+}]$ spikes are also delivered to the mitochondria to control the activity of several enzymes that participate in ATP production as well as that of other proteins compartmentalized to the matrix space (19–21). Mitochondrial Ca^{2+} uptake sites display low affinity toward Ca^{2+} and appear to respond mostly to the large local $[Ca^{2+}]_c$ transients that occur in the vicinity of the activated IP3Rs and RyRs (21–24), but a rapid mode of Ca^{2+} uptake at relatively low $[Ca^{2+}]$ has also been documented (25). A local interaction between RyRs and mitochondrial Ca^{2+} uptake sites may secure that even fundamental Ca^{2+} release events (Ca^{2+} sparks) induce a $[Ca^{2+}]_m$ increase in the neighboring mitochondrion (Ca^{2+} mark) (26). However, a substantially larger $[Ca^{2+}]_m$ rise occurs during a global $[Ca^{2+}]_c$ signal, suggesting that numerous Ca^{2+} release events cooperate with each other to establish a $[Ca^{2+}]_m$ signal in a mitochondrion. At the ER-mitochondrial interface, great quantities of IP3Rs have been visualized and enrichment in ER Ca^{2+} pumps and mitochondrial Ca^{2+} uniporters is probable (reviewed in Refs. 27 and 28). Morphology of the ER-mitochondrial associations and concentration of the Ca^{2+} transporters at the interface may play a role in controlling coordinated activation of the individual Ca^{2+} release events that give rise to the IP_3-linked $[Ca^{2+}]_m$ spikes. Thus, the role of IP_3 in coordination of Ca^{2+} release events is of great interest in a variety of Ca^{2+} signaling mechanisms. We reasoned that mobile IP_3 buffers should be useful to test the role of IP_3 in $[Ca^{2+}]_c$ wave propagation, activation of Ca^{2+} entry, and in IP3R-dependent activation of mitochondrial Ca^{2+} uptake.

An intensely investigated IP_3-binding module is the IP_3-binding domain of the IP3R. The N-terminal cytoplasmic region of the human type-I IP3R (residues 1–604) binds IP_3 with comparable affinity to the full-length IP3R (29). Removal of residues 1–223 (suppressor region) further increases the affinity for IP_3 (30). Expression of $IP_3R_{224-605}$ has been shown to attenuate the ATP-induced $[Ca^{2+}]_c$ signal in human embryonic kidney 293 and in COS-7 cells (31, 32). Another structurally unrelated IP_3-binding module is the PH domain of certain proteins. Some PH domains are known to bind IP_3 and/or PIP_2, for example, the PH domains of PLCδ1 and the PLC-like 130-kDa protein (p130). p130 was isolated from rat brain as an IP3BP (33) and has been shown to be important in the signaling by $GABA_A$ receptors (34). p130 shares 38.2% sequence homology to PLC-δ1 but lacks catalytic activity. The PH domain of p130 (residues 95–233) has also been shown to inhibit the $[Ca^{2+}]_c$ signal evoked by IP_3-linked agonists (31, 35).

Our main objective was to evaluate the possible role of fluctuations of IP_3 in the spatio-temporal organization of the calcium signal, utilizing $IP_3R_{224-605}$ and p130PH. Our results indicate that these two proteins are freely distributed in the cytosol, inhibit Ca^{2+} release induced by suboptimal IP_3 but do not suppress Ca^{2+} release evoked by sensitization of the IP3R to IP_3, and fail to attenuate non-IP3R-mediated Ca^{2+} release. Thus, $IP_3R_{224-605}$ and p130PH act as mobile cytosolic IP_3 buffers. $IP_3R_{224-605}$ and p130PH were used next to explore the effects of IP_3 buffering on the propagation of IP_3-linked $[Ca^{2+}]_c$ waves, store depletion-induced Ca^{2+} entry, and on $[Ca^{2+}]_c$ signal propagation to the mitochondria. Our studies reveal that buffering of IP_3 leads to a decrease in the velocity of $[Ca^{2+}]_c$ waves and can effectively uncouple $[Ca^{2+}]_m$ from the $[Ca^{2+}]_c$ signal in the cell.

EXPERIMENTAL PROCEDURES

DNA Constructs and Recombinant Proteins—The constructs encoding the fusion proteins of the PH domain of $PLC\delta_1$ or of the p130 protein and the (1,4,5)IP_3-binding domain (residues 224–605) of the human type-I (1,4,5)IP_3 receptor with cyan, green, or yellow fluorescent protein have been described previously (31). In addition, the PH domain of p130 and the R134L mutant were also inserted into a plasmid encoding a monomeric red fluorescent protein (RFP-p130PH and RFP-p130PH-R134L) (36). Ratiometric pericam targeted to the mitochondria (pericam-mt) has also been published previously (37). Bacterial expression of the GFP-fused protein domains (p130PH-GFP, GFP-$IP_3R_{224-605}$, and GFP-PLCδ1PH R40L) was carried out as described previously (31).

Cell Culture—COS-7 cells (obtained from ATCC) were cultured in Dulbecco's modified essential medium supplemented with 10% fetal bovine serum, 100 units/ml penicillin, and 100 μg/ml streptomycin in humidified air (5% CO_2) at 37 °C. RBL-2H3 cells were cultured as described previously (22). For imaging experiments, cells were plated onto poly-D-lysine-treated glass coverslips at a density of 20,000–25,000/cm^2 and were grown for 3–4 days. For cell suspension studies, cells were cultured for 4–6 days in 75-cm^2 flasks.

Transfection of Cells—Cells plated onto poly-D-lysine-coated coverslips were transfected with plasmid DNA (1.5 μg/ml) for 6–12 h using Lipofectamine (Invitrogen) and Opti-MEM I medium (Invitrogen) according to the manufacturer's instructions. Cells were observed 24–36 h after transfection.

Measurement of [^{3}H]IP_3—COS-7 cells (5×10^4 cells/ml) were cultured on 12-well culture dishes for 1 day and transfected with either the RFP-p130PH or RFP-p130PH-R134L construct. After 24 h, cells were labeled in 0.75-ml inositol-free Dulbecco's modified essential medium containing 0.1% BSA, 2.5% fetal bovine serum, and *myo*-[^{3}H]inositol (20 μCi/ml, Amersham Biosciences) for 24 h. After two washes, cells were preincubated for 30 min at 37 °C before stimulation with 50 μM ATP for the indicated times. Incubations were terminated by the addition of ice-cold perchloric acid (5% final). Inositol phosphates were extracted and separated on high pressure liquid chromatography as described previously (38). The (1,4,5)IP_3 and (1,3,4)IP_3 values were combined.

Fluorescence Imaging Measurements in Intact COS-7 Cells—Before use, the cells were preincubated in an extracellular medium (2% BSA/ECM) consisting of 121 mM NaCl, 5 mM $NaHCO_3$, 10 mM Na-HEPES, 4.7 mM KCl, 1.2 mM KH_2PO_4, 1.2 mM $MgSO_4$, 2 mM $CaCl_2$, 10 mM glucose, and 2% BSA, pH 7.4. To monitor $[Ca^{2+}]_c$ and to measure Mn^{2+} entry (Mn^{2+} quench), cells were loaded with 5 μM Fura-2/AM for 20–30 min in the presence of 200 μM sulfinpyrazone and 0.003% (w/v) pluronic acid at room temperature. Sulfinpyrazone was also present during the imaging measurements to minimize dye loss. To monitor $[Ca^{2+}]_m$, cells were loaded with 5 μM rhod2/AM for 50 min in the presence of 0.003% (w/v) pluronic acid at 35 °C. After loading, cells were washed and incubated in the same medium containing 0.25% BSA but no Ca^{2+} tracer was added. In some experiments, Ca^{2+} was not added to 0.25% BSA/ECM and the final $[Ca^{2+}]_{ECM}$ was <1 μM.

Coverslips were mounted at the thermostated stage (35 °C) of an Olympus IX70 inverted microscope fitted with a ×40 (UApo, NA 1.35) oil immersion objective. For simultaneous measurements of fura2, pericam, and RFP fluorescence, a Leica IRB2 inverted microscope equipped with a motorized turret under computer control and fitted with the above described objective was used. Fluorescence images were collected using a cooled CCD camera (PXL, Photometrics or, for fast-imaging, a frame-transfer device, Pluto, PixelVision) (22, 31, 39). The following multi-parameter imaging protocols were applied: fura2 and GFP (fura2, 340- and 380-nm excitations or 360 nm for Mn^{2+} quenching; enhanced GFP, 490-nm excitation, 510-nm longpass dichroic mirror, and a 520-nm longpass emission filter); CFP and YFP (CFP, 435-nm excitation, 480/40-nm emission; FRET, 435-nm excitation, 535/30-nm emission); and fura2, pericam, and RFP (fura2, 340- and 380-nm excitation; pericam, 414- and 495-nm excitation, 510-nm longpass dichroic mirror, and a 520-nm longpass emission filter; RFP, 545-nm excitation, 570-nm longpass dichroic mirror, and a 603/75-nm emission filter; CCD imaging system). In most of the experiments, a set of images was obtained every 3 s, whereas in recording of the waves 15 frames were obtained in each second, and in the measurements that involved a switch of the filter cube in each cycle, a set of images was obtained every 6 s.

For evaluation of $[Ca^{2+}]_c$, fura2 fluorescence was calculated for the total area of individual cells and the background fluorescence obtained over cell-free regions of each image was subtracted prior to calculation of the fluorescence ratios. In the cells expressing high amounts of fluorescent proteins, detectable GFP/pericam fluorescence was obtained at the excitation wavelengths used for fura2 (40). The GFP-related fluorescence was not affected by changes in $[Ca^{2+}]_c$. Although a comparison of the fura2 fluorescence between fluorescent protein-expressing cells and non-transfected cells was used to visualize the kinetics of the signal in each image sequence, to avoid underestimation of the

fluorescence ratios reflecting the changes in $[Ca^{2+}]_c$, GFP-N *versus* p130PH-GFP or GFP-IP$_3$R$_{224-605}$ and RFP-N *versus* RFP-p130PH were also analyzed in all of the comparisons. For evaluation of $[Ca^{2+}]_m$, the pericam-mt signal was masked. Recordings obtained from all of the transfected cells on the field were averaged for comparison in each experiment. Experiments were carried out with at least four different cell preparations, and 20–60 cells were monitored in each experiment. Significance of differences from the relevant controls was calculated by Student's *t* test.

Confocal Imaging of Fluorescence Recovery after Photobleaching (FRAP) Measurements in COS-7 Cells—COS-7 cells were transfected with GFP-N, GFP-IP$_3$R$_{224-605}$, p130PH-GFP, mito-YFP, or PLCδ_1PH-GFP. Experiments were performed in 0.25% BSA at 35 °C. A Bio-Rad Radiance 2100 confocal laser-scanning system coupled to an Olympus IX70 inverted microscope with a ×40 (UApo, NA 1.35) oil immersion objective was used to record image series. The 488-nm line of a krypton/argon laser was used to excite the GFP. For the FRAP measurements, images were taken continuously at 512 × 512 resolution at a high digital zoom (0.1 μm/pixel) with a frame rate of 0.3 Hz. Two 64 μm^2 (80 × 80 pixels) regions were selected for bleaching. Two images were recorded pre-bleach followed by five bleaching images with the selected regions illuminated at 16.7 (GFP-N) and 25 times (GFP-IP$_3$R$_{224-605}$, p130PH-GFP, and mito-YFP) the normal scanning intensity. The cell was scanned continuously for 5.5 min after bleaching.

Measurement of $[Ca^{2+}_c]$ in Suspension of Permeabilized COS-7 Cells—Cells harvested using 0.25% trypsin were washed in an ice-cold Ca^{2+}-free extracellular buffer containing 120 mM NaCl, 5 mM KCl, 1 mM KH_2PO_4, 0.2 mM $MgCl_2$, 0.1 mM EGTA, and 20 mM HEPES-NaOH, pH 7.4. Equal aliquots of cells (10–12 ×10^6 cells) were resuspended and permeabilized with 40 μg/ml digitonin in 1.4 ml of an intracellular medium (ICM) composed of 120 mM KCl, 10 mM NaCl, 1 mM KH_2PO_4, and 20 mM HEPES-Tris, pH 7.2, supplemented with 1 μg/ml each of antipain, leupeptin, and pepstatin A. ICM was passed through a Chelex column prior to the addition of protease inhibitors to lower the ambient $[Ca^{2+}]$. All of the measurements were carried out in the presence of 2 mM MgATP and 2 mM succinate. Cytosolic $[Ca^{2+}]$ was measured using fura2/FA (0.5 μM, excitation 340 and 380 nm; emission, 500 nm) added to the incubation medium. For GFP, 490-nm excitation and 535-nm emission were used. Fluorescence was monitored in a multi-wavelength-excitation dual wavelength-emission fluorimeter (Delta RAM, PTI). Incubations were carried out at 35 °C in a stirred thermostated cuvette. Calibration of fura2 signal was carried out at the end of each measurement by adding 1.5 mM $CaCl_2$ and subsequently 10 mM EGTA-Tris, pH 8.5. $[Ca^{2+}]_c$ was calculated using a K_d of 224 nM.

Fluorometric Measurements of $[Ca^{2+}]_c$ and $[Ca^{2+}]_m$ in Suspensions of Permeabilized RBL-2H3 Cells—Measurements were carried out as described before (22, 41). fura2FF-loaded cells (5.5 × 10^6 cells/ml) were permeabilized in ICM supplemented with 25–35 μg/ml digitonin for 5 min at 35 °C followed by washout of the released cytosolic fura2FF (125 × *g* for 4 min). Cell permeabilization was evaluated by trypan blue exclusion, and after a 5-min incubation, >95% cells were trypan blue-positive. Compartmentalized fura2FF has been shown to occur in the mitochondria of RBL-2H3 cells. Permeabilized cells were resuspended in ICM supplemented with succinate 2 mM and 0.25 μM rhod2/FA and maintained in a stirred thermostated cuvette at 35 °C. Rhod2/FA was added to monitor $[Ca^{2+}]$ in the intracellular medium that exchanges readily with the cytosolic space. Fluorescence was monitored in a multi-wavelength-excitation dual wavelength-emission fluorimeter using 340- and 380-nm excitation and 500-nm emission for fura2FF and 540-nm excitation and 580-nm emission for rhod2. In every experiment, five data triplets were obtained per second. Calibration of the Ca^{2+} signals was carried out at the end of each measurement as described previously (41).

RESULTS AND DISCUSSION

Cellular Localization of IP$_3$- and Inositol Lipid-binding Domains Fused to GFP—We first visualized by confocal microscopy the subcellular localization of the IP$_3$-binding domains, IP$_3$R$_{224-605}$ and p130PH, in COS-7 cells, which were expressed as GFP fusion proteins. GFP-N was used as a control for cytosolic distribution (Fig. 1*A*, *i*), whereas PLCδ_1PH-GFP that binds to PIP$_2$ through its PH domain was used as a reference for plasma membrane localization (Fig. 1*A*, *iv*). As indicated by the GFP fluorescence, GFP-IP$_3$R$_{224-605}$ and p130PH-GFP were found to be present in the cytoplasm (Fig. 1*A*, *ii* and *iii*). The cells were stimulated next with ATP that induces PLC-mediated cleavage of PIP$_2$ to enhance IP$_3$ formation. In ATP-stimulated COS-7 cells, no change was observed in the distribution of GFP-N, GFP-IP$_3$R$_{224-605}$, and p130PH-GFP (Fig. 1*A*, *v*, *vi*, and *vii*). The ATP-induced hydrolysis of PIP$_2$ was confirmed by the partial translocation of PLCδ_1PH-GFP from the membrane to the cytosol, which appeared as a fluorescence decrease at the plasma membrane and an increase in the cytosol (Fig. 1*A*, *viii*).

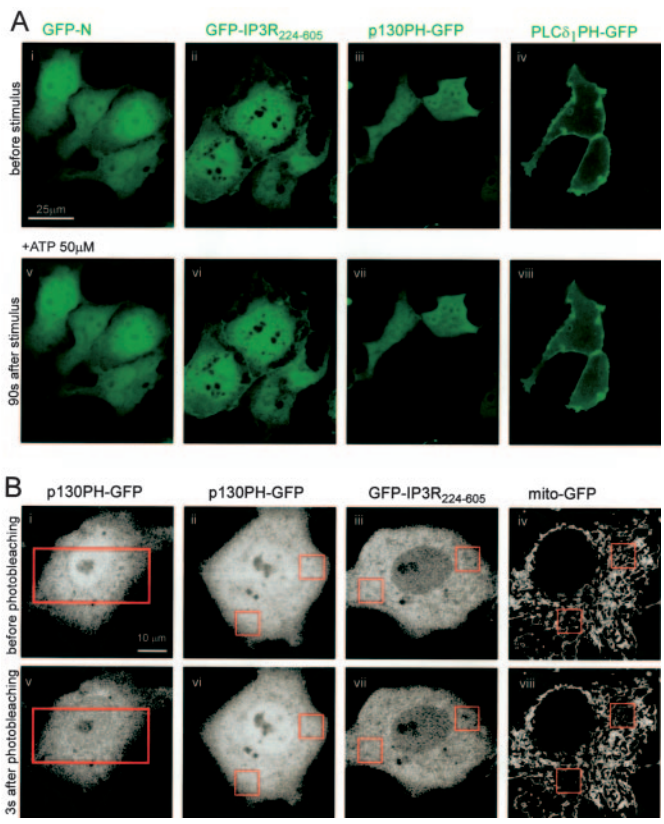

FIG. 1. **Subcellular distribution and mobility of inositol lipid- and IP$_3$-binding domains fused to GFP in COS-7 cells.** *A*, confocal images of COS-7 cells transfected with constructs encoding the PH domain of the p130, the N-terminal ligand-binding domain of the IP$_3$R$_{224-605}$, or the PH domain of the PLCδ_1 fused to GFP. Images were recorded before (*upper panel*) and 90 s after the addition of 50 μM ATP (*lower panel*). *B*, confocal images from a FRAP experiment with COS-7 cells transiently transfected with p130PH-GFP (*i*, *ii*, *v*, and *vi*), GFP-IP$_3$R$_{224-605}$ (*iii* and *vii*), and YFP targeted to the mitochondrial matrix via a fusion with the targeting sequence of cytochrome *c* oxidase subunit VIII (mito-GFP, *iv* and *viii*). Pre-bleach is shown in the *upper row*, and immediately post-bleach (3.3 s) is shown in the *lower row*. The bleaching regions are marked by a *red box*.

FRAP studies were used to assess the mobility of the IP3BPs in the cytosol (Fig. 1*B*). When a large area of a p130PH-GFP-expressing cell was illuminated, an essentially homogeneous decrease in fluorescence appeared throughout the cell within 3s (Fig. 1*B*, *i versus v*), suggesting fast cytosolic distribution of the fluorescent protein. Furthermore, when small regions of the GFP-IP$_3$R$_{224-605}$-and p130PH-GFP-expressing cells were photobleached, the post-bleach fluorescence in these regions was not different from the pre-bleach signal, indicating that the fluorescence was recovered completely within 3s (Fig. 1*B*, *ii versus vi* and *iii versus vii*). As a positive control, GFP targeted to the mitochondrial matrix, mito-GFP, which shows slower redistribution than the cytosolic GFP (42), was also photobleached. In this case, the loss of fluorescence in the region of bleaching was apparent in the post-bleach image (Fig. 1*B*, *iv versus* viii; 29 ± 3%, n = 12). Although the rate of image acquisition was too low to determine the half-recovery time for GFP-IP$_3$R$_{224-605}$ and p130PH-GFP, it is likely to be in the

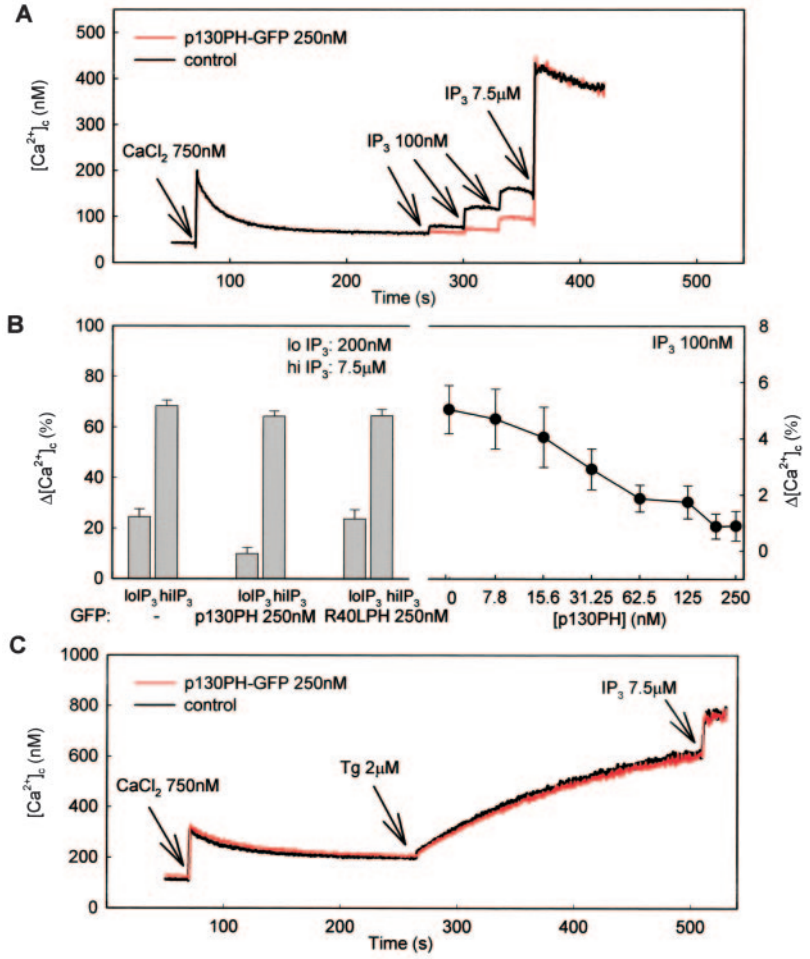

FIG. 2. **Effect of recombinant p130PH-GFP on IP$_3$-induced Ca^{2+} release in permeabilized COS-7 cells.** Ca^{2+} accumulation and release by permeabilized COS-7 cells were monitored in a fluorometer using the ratiometric Ca^{2+} indicator, fura2/FA. *A*, cells were first subjected to a 750 nM $CaCl_2$ pulse that optimized the Ca^{2+}-loading state of the ER and then exposed to sequential 100 nM IP$_3$ additions followed by a 7.5 μM IP$_3$ challenge. p130PH-GFP (*red*) or solvent (*black*) was added at the beginning of each run. *B*, *left*, various concentrations of IP$_3$ (200 nM and 7.5 μM) were added to cells in the absence or presence of p130PH-GFP and GFP-R40LPH. The IP$_3$-induced increase in [Ca^{2+}]$_c$ was normalized to the [Ca^{2+}]$_c$ change caused by ionomycin (10 μM) (mean ± S.E., n = 8). *Right*, dose response relation for the inhibition of 100 nM IP$_3$ induced [Ca^{2+}]$_c$ increase by p130PH-GFP. Each point represents the mean of at least 2–3 measurements. *C*, after preloading the ER with a 750 nM $CaCl_2$ pulse, 2 μM Tg and subsequently 7.5 μM IP$_3$ were added. The data are representative of experiments repeated at least three times.

subsecond range, similarly to the half-recovery time measured for a freely diffusible cytosolic PH domain-GFP construct (PLCδ1PH(R40L)-GFP, 0.2s) (43). Collectively, the above data suggest that the GFP-IP$_3$R$_{224-605}$ and p130PH-GFP are highly mobile cytosolic proteins.

Suppression of IP$_3$-induced Ca^{2+} Release by p130PH-GFP and GFP-IP$_3$R$_{224-605}$ in Permeabilized Cells—To evaluate the extent to which the GFP-fused IP$_3$-binding domains can buffer IP$_3$ in the cytoplasm, we analyzed the effect of recombinant p130PH-GFP on IP$_3$-induced Ca^{2+} release in permeabilized COS-7 cells (Fig. 2*A*). The change of [Ca^{2+}] in the cytosolic buffer ([Ca^{2+}]$_c$) was monitored by fura2. First, a Ca^{2+} pulse (750 nM $CaCl_2$) was added to the permeabilized cells. The added Ca^{2+}-induced [Ca^{2+}]$_c$ rise and subsequent rapid decay were not affected by the presence of p130PH-GFP (250 nM), indicating that cytoplasmic Ca^{2+} buffering and the ER Ca^{2+} uptake were not influenced by p130PH-GFP (Fig. 2*A*, *red versus black line*). After a steady state [Ca^{2+}]$_c$ was attained, submaximal IP$_3$ was added in three steps, 100 nM each, followed by the addition of a supramaximal dose (7.5 μM). The three additions of 100 nM IP$_3$ triggered a dose-dependent increase in [Ca^{2+}]$_c$, and the supramaximal IP$_3$ evoked an additional large [Ca^{2+}]$_c$ increase (Fig. 2*A*). When recombinant p130PH-GFP was present, the [Ca^{2+}]$_c$ rise elicited by the suboptimal IP$_3$ was largely attenuated but the [Ca^{2+}]$_c$ change in response to maximum IP$_3$ dose was not affected (Fig. 2*A*, *red versus black line*). On average, >50% inhibition of the [Ca^{2+}]$_c$ signal evoked by 200 nM IP$_3$ was obtained in the presence of p130PH-GFP (250 nM), whereas no inhibition was caused by the GFP fusion protein of PLCδ$_1$PH R40L, a PLCd$_1$PH mutant that does not bind IP$_3$ (Fig. 2*B*, *left*) (31). The dose response relation also showed highly effective inhibition of the IP$_3$-induced [Ca^{2+}]$_c$ signal by p130PH-GFP (Fig. 2*B*, *right*). Similar to p130PH-GFP, GFP-IP$_3$R$_{224-605}$ (50 nM) also inhibited the [Ca^{2+}]$_c$ signal induced by 100 nM IP$_3$ (40% inhibition) and failed to affect the [Ca^{2+}]$_c$ response elicited by 7.5 μM IP$_3$ (not shown, n = 2). These results suggest that p130PH-GFP and GFP-IP$_3$R$_{224-605}$ were able to compete with the IP3R for IP$_3$ until IP$_3$ was available for saturation of both the IP3R and the recombinant IP3BPs. As compared with IP$_3$, Tg (2 μM), an inhibitor of the ER Ca^{2+} pumps, induced a slow but progressive [Ca^{2+}]$_c$ rise that was mediated by Ca^{2+} leak from the ER (Fig. 2*C*). p130PH-GFP did not affect the Tg-induced [Ca^{2+}]$_c$ signal, suggesting that the ER Ca^{2+} leak was not controlled by p130PH-GFP (Fig. 2*C*). Thus, IP$_3$-binding domains attenuated selectively the IP3R-mediated Ca^{2+} release from the ER.

Effect of IP$_3$-binding Domains on the [Ca^{2+}]$_c$ Signal Evoked by IP$_3$-linked Agonists in Intact Cells—To further analyze the effect of p130PH and IP$_3$R$_{224-605}$ on Ca^{2+} signaling, agonists activating PLCβ or PLCγ were added to intact COS-7 cells expressing either p130PH-GFP or GFP-IP$_3$R$_{224-605}$. Microscopic imaging of GFP fluorescence (490-nm excitation) simultaneously with fura2 fluorescence (340- and 380-nm excitation) allowed us to evaluate the agonist-induced [Ca^{2+}]$_c$ signal both in transfected and non-transfected (control) cells (Fig. 3). ATP (50 μM) that activates PLCβ through P2-purinergic receptors elicited a robust and rapid global [Ca^{2+}]$_c$ elevation in control cells (Fig. 3, *A* and *B*, *50- versus 66-s image*). In contrast, the GFP-positive cells (Fig. 3, *A* and *B*, *GFP image*) did not exhibit a [Ca^{2+}]$_c$ rise or displayed only a delayed response (Fig. 3, *A*, *GFP-IP$_3$R$_{224-605}$*, *120-s image*, and *B*, *p130PH-GFP*, *81-s image*). The mean response of the control cells showed a steep and

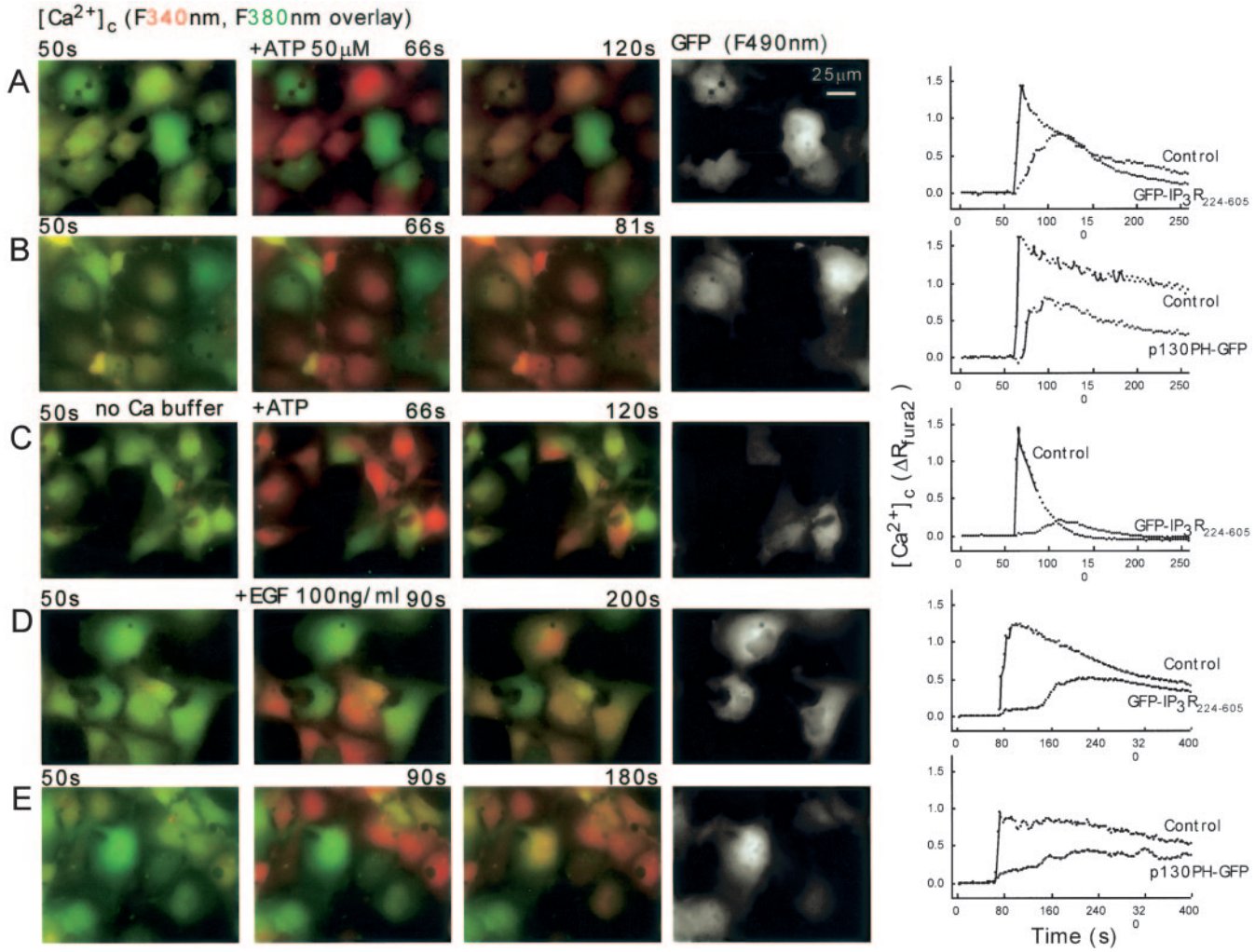

FIG. 3. **Inhibition of the global $[Ca^{2+}]_c$ response to IP_3-linked agonists by GFP-$IP_3R_{224-605}$ and by p130PH-GFP in intact COS-7 cells.** *A–E*, single cell $[Ca^{2+}]_c$ imaging with fura2 was carried out in cells transfected with constructs encoding GFP-$IP_3R_{224-605}$ (*A*, *C*, and *D*) or p130PH-GFP (*B* and *E*). $[Ca^{2+}]_c$ increase is shown by a *green* to *red shift* in the overlay of the *green* (excited at 380 nm) and *red* (excited at 340 nm) *images*. GFP fluorescence was detected at a 490-nm excitation. Cells were stimulated with ATP (50 μM; *A* and *B*, in the presence of extracellular calcium, and *C* in the absence of extracellular calcium) or EGF (100 ng/ml; *D* and *E*). Mean time courses of $\Delta[Ca^{2+}]_c$ calculated for the GFP-positive and negative (*control*) cells, respectively, are shown in the graphs. The data are representative of experiments repeated at least five times.

massive $[Ca^{2+}]_c$ rise as observed in the individual cells (Fig. 3, *graphs* in *A* and *B*), whereas the mean response of the GFP-$IP_3R_{224-605}$ cells and p130PH-GFP cells showed a slower ATP-induced $[Ca^{2+}]_c$ increase (Fig. 3*A* graph and Fig. 3*B* graph, respectively). To determine the effect of the IP_3-binding domains on ATP-induced Ca^{2+} mobilization, stimulation of the cells was also carried out in Ca^{2+}-free bathing medium (Fig. 3*C*). In the absence of extracellular Ca^{2+}, ATP induced a rapidly rising and decaying $[Ca^{2+}]_c$ spike in control cells and a delayed and relatively small $[Ca^{2+}]_c$ increase in GFP-$IP_3R_{224-605}$-expressing cells (Fig. 3*C*). This result further supports that the ATP-stimulated Ca^{2+} mobilization was effectively inhibited in the presence of the IP_3-binding domain of the IP3R. EGF (100 ng/ml) that promotes PLCγ-mediated IP_3 formation also elicited a large $[Ca^{2+}]_c$ signal in control cells, which was delayed as compared with the ATP-induced $[Ca^{2+}]_c$ signal (Fig. 3, *D* and *E*, note the different time scales in *panels A–C* and *D* and *E*). Nevertheless, the expression of GFP-$IP_3R_{224-605}$ (Fig. 3*D*) or p130PH-GFP (Fig. 3*E*) resulted in further extension of the lag time and smaller magnitude of the EGF-stimulated $[Ca^{2+}]_c$ rise.

To quantitate the effect of expression of cytosolic IP_3-binding domains on the generation of the $[Ca^{2+}]_c$ signal, we counted the cells that failed to respond to the agonist and, in the responsive cells, measured the lag time of the $[Ca^{2+}]_c$ signal (t_{lag}), the fura2 ratio before stimulation (R_0), the change in R_{fura2} during the $[Ca^{2+}]_c$ signal (ΔR), and the mean GFP fluorescence (F_{GFP}) (Table I). In addition to the cells that did not express GFP-$IP_3R_{224-605}$ or p130PH-GFP, cells transfected with GFP-N were also used as a control. Both the fraction of cells that did not respond to agonist and the lag time of the $[Ca^{2+}]_c$ signal were similar in GFP-N cells to that in non-transfected cells (Table I). Notably, R_0 and ΔR for any of the agonists were smaller in GFP-N cells than in non-transfected cells (Table I). This result is likely to reflect a bleed through the bright F_{GFP} to the records of the fura2 fluorescence (in particular to F_{380}) in the GFP-N cells (Table I). Thus, the cross-talk between GFP and fura2 fluorescence could also contribute to the small ΔR obtained in GFP-$IP_3R_{224-605}$ or p130PH-GFP-expressing cells. However, both F_{GFP} and ΔR were larger in GFP-N cells than in GFP-$IP_3R_{224-605}$ or p130PH-GFP cells (Table I), suggesting that the IP_3-binding domains caused a decrease in the magnitude of the $[Ca^{2+}]_c$ signal. Table I also shows that the $[Ca^{2+}]_c$ evoked by bradykinin, another agonist of the PLCβ pathway, was also delayed and decreased by GFP-$IP_3R_{224-605}$, whereas the $[Ca^{2+}]_c$ rise induced by Tg was not affected by GFP-$IP_3R_{224-605}$ (Table I). When compared with non-transfected cells, the GFP-$IP_3R_{224-605}$- or p130PH-GFP-expressing cells showed an apparent attenuation of both the initial and the

TABLE I
Effect of GFP fused IP3BPs on global $[Ca^{2+}]_c$ signaling in intact COS-7 cells

Cells transfected with GFP-N, p130PH-GFP, or GFP-$IP_3R_{224-605}$ were stimulated with Ca^{2+}-mobilizing agonists as follows: 50 μM ATP; 100 ng/ml EGF; 200 nM bradykinin (BK); and 2 μM thapsigargin in the presence or absence of 2 mM $CaCl_2$ in the extracellular medium ($+Ca^{2+}$ or $-Ca^{2+}$). No.(S/T), the silent cell numbers (cell without response) *versus* total cell numbers; a.u., arbitrary units. The results of 12 fluorescence-imaging experiments cells were summarized.

		Control	GFP-N	p130PH-GFP	GFP-$IP_3R_{224-605}$
ATP $+Ca^{2+}$	t_{lag} (S)	4.7 ± 0.2	3.6 ± 0.2	17.8 ± 2.1	39.7 ± 3.0
	No.(S/T)[a]	3/806	2/194	16/123	13/200
	R_0/R_P	0.64/1.96	0.47/1.01	0.47/0.75	0.55/0.97
	F_{GFP} (a.u.)		3593 ± 191	2986 ± 179	2062 ± 116
ATP $-Ca^{2+}$	t_{lag} (S)	3.7 ± 0.4	3.3 ± 0.3		21.4 ± 3.5
	No.(S/T)	4/90	0/90		5/64
	R_0/R_P	0.6/1.56	0.41/0.86		0.49/0.82
	F_{GFP} (a.u.)		5266 ± 300		2448 ± 253
EGF	t_{lag} (S)	39.1 ± 2.9	31.9 ± 4.2	130.1 ± 7.1	152.8 ± 11.7
	No.(S/T*)	11/202	2/78	20/120	10/69
	R_0/R_P	0.68/1.39	0.57/0.95	0.56/0.86	0.6/1.0
	F_{GFP} (a.u.)		3437 ± 191	4078 ± 275	1985 ± 137
BK	t_{lag} (S)	14.5 ± 1.3	16.8 ± 2.5		35.9 ± 7.8
	No.(S/T*)	23/181	5/40		10/23
	R_0/R_P	0.63/1.68	0.51/0.87		0.63/0.83
	F_{GFP} (a.u.)		3113 ± 234		1266 ± 160
Tg $+Ca^{2+}$	t_{lag} (S)		17.4 ± 1.3		23.4 ± 2.6
	No.(S/T*)		0/57		0/37
	R_0/R_P		0.38/0.5		0.49/0.7
	F_{GFP} (a.u.)		5266 ± 300		2448 ± 253
Tg $-Ca^{2+}$	t_{lag} (S)	14.5 ± 0.6	13.7 ± 0.4		15.3 ± 0.5
	No.(S/T*)	0/267	0/129		0/113
	R_0/R_P	0.59/1.05	0.52/0.71		0.53/0.72
	F_{GFP} (a.u.)		4750 ± 213		3148 ± 211

sustained phases of the ATP- and EGF-induced $[Ca^{2+}]_c$ signal (Fig. 3, *A*, *B*, *D*, and *E*). However, the difference in the sustained phase is not a reflection of the inhibition of Ca^{2+} entry because no difference in the sustained phase was observed when the GFP-$IP_3R_{224-605}$ or p130PH-GFP-expressing cells were compared with GFP-expressing cells (see below, Fig. 6, *A* and *B*). Taken together, these data show that the expression of IP_3-binding domains suppress $[Ca^{2+}]_c$ signaling that is dependent on IP_3 formation and IP3R-mediated Ca^{2+} mobilization. By contrast, no effect appeared on $[Ca^{2+}]_c$ elevation that was dependent on non-IP3R-mediated discharge of the ER.

After showing that the IP3R-mediated Ca^{2+} mobilization is effectively inhibited by the recombinant IP3BPs (Fig. 2), their effect on the IP_3 formation was tested (Fig. 4). Because only a small fraction of the transfected cells expressed GFP-$IP_3R_{224-605}$ ($\leq$20% efficacy) and no single-cell IP_3 assay was available, we determined the basal and agonist-stimulated total $[IP_3]$ in cells transfected with p130PH-GFP (~50% efficacy) or its mutant form unable to bind IP_3. The basal and ATP-stimulated $[^3H]IP_3$ levels were ~20 and 40% higher, respectively, in the p130PH-GFP-transfected cells (Fig. 4). After correction for transfection efficiency, the p130PH-GFP-expressing cells showed ~40 and 80% increase in the basal and ATP-stimulated $[^3H]IP_3$ levels, respectively. This result suggests that the buffering effect of p130PH-GFP brought about a compensatory increase in total IP_3, enabling the cells to keep the basal-free IP_3 levels close to normal and to show an $[IP_3]$ signal during stimulation by an agonist. Although the total IP_3 formation was increased, the IP3BPs would have suppressed the free $[IP_3]$ rise to attenuate the IP_3-linked $[Ca^{2+}]_c$ signal.

Based on the above results, the cytosolic IP3BPs may serve as mobile cytosolic IP_3-buffers, providing a novel means to study the role of $[IP_3]$ elevation in calcium signaling phenomena that have been proposed to depend on regenerative activation of the IP3Rs (*e.g.* $[Ca^{2+}]_c$ wave propagation) or to depend on local interactions between IP3R and other Ca^{2+} channels (*e.g.* activation of store depletion-induced Ca^{2+} entry and Ca^{2+} signal delivery to the mitochondria).

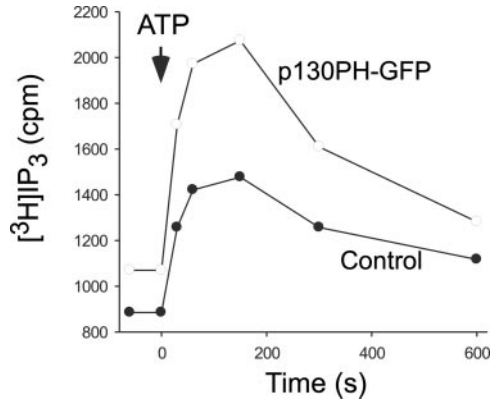

FIG. 4. **Effect of the IP3BPs on the basal and ATP-stimulated $[^3H]IP_3$ formation.** Time course of total cellular $[^3H]IP_3$ in cells transfected with p130PH-GFP or RFP-p130PH-R134L (*control*). The data are representative of experiments carried out in duplicates and repeated twice.

Effect of Cytosolic IP3BPs on $[Ca^{2+}]_c$ Wave Propagation—To track the spatio-temporal pattern of the ATP-induced $[Ca^{2+}]_c$ signal, we carried out fast recording of fura2 fluorescence (F_{380}, 15 frames/s) in control and GFP-$IP_3R_{224-605}$-expressing COS-7 cells (Fig. 5). To visualize the sites of the $[Ca^{2+}]_c$ rise, $F_{380\ nm}$ images were differentiated through time (ΔF, *purple overlay* on *gray-scale images*). In each of the four control cells surrounding the GFP-$IP_3R_{224-605}$-expressing cell (in the *center*), the $[Ca^{2+}]_c$ rise started in one region and spread throughout the whole cells in 0.6 s or less (Fig. 5, *time series* of $\Delta F/F380$ *images*). In cells expressing GFP-$IP_3R_{224-605}$, the onset of the $[Ca^{2+}]_c$ rise was delayed as described above, and although the $[Ca^{2+}]_c$ signal still appeared as a $[Ca^{2+}]_c$ wave, its propagation was much slower than that in control cells (Fig. 5, *lower two rows* of *images*). Direction of the $[Ca^{2+}]_c$ wave is marked by *arrows* for two control cells and a GFP-$IP_3R_{224-605}$-expressing cell (*upper row*, *right*), and for three regions selected along the wave propagation, the time course of the $[Ca^{2+}]_c$ rise (decrease in F_{380} fluorescence) is shown (Fig. 5, *right*; *control*, *upper* and *middle*;

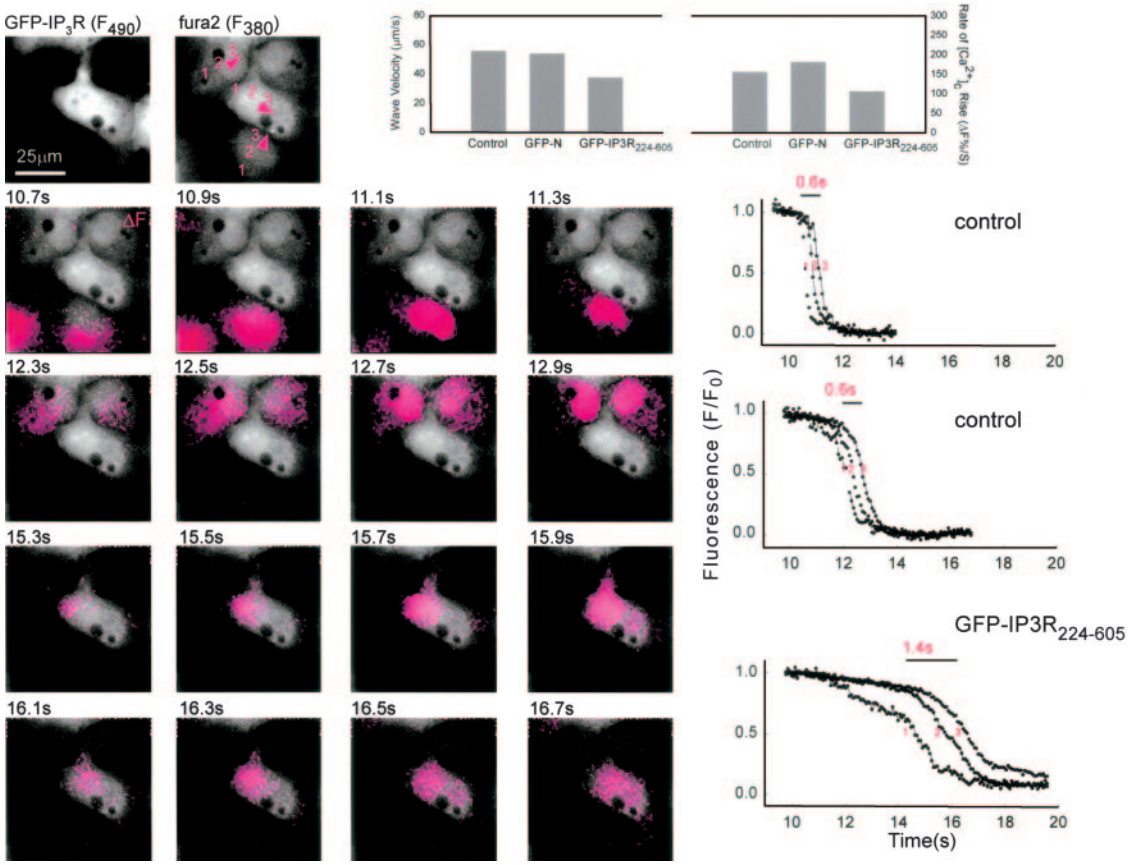

FIG. 5. **Effect of GFP-IP$_3$R$_{224-605}$ on propagation of IP$_3$-linked [Ca^{2+}]$_c$ waves through COS-7 cells.** Cells were transfected with GFP-IP$_3$R$_{224-605}$ and loaded with fura2 as described in Fig. 3 legend. To evaluate the spatial pattern of [Ca^{2+}]$_c$ waves evoked by ATP (50 μM), images were acquired at 15 frames/s at 380-nm excitation. The *purple overlays* show the fluorescence decrease at each time point and thus represent the spatial localization of the [Ca^{2+}]$_c$ increases within the cells. In the *upper right image*, *arrows* indicate the directions of wave propagation. In addition, an image was acquired at 490-nm excitation to visualize the GFP-IP$_3$R$_{224-605}$-expressing cells (*upper left*). In the *graphs* on the *right*, time courses of the changes in F_{380} are shown at subregions of the cells (*marked* by *purple numbers*) selected along the direction of the wave propagation for each cell. *Upper graph*, the velocity of wave propagation (*left*) and the rate of [Ca^{2+}]$_c$ rising phase (*right*) are shown (mean ± S.E. $n = 6$).

GFP-IP$_3$R$_{224-605}$, lower panel). The traces show that both the rising phase of the [Ca^{2+}]$_c$ spike at each subcellular region and the rate of traveling of the [Ca^{2+}]$_c$ signal from one region to the next were relatively slow in the GFP-IP$_3$R$_{224-605}$-expressing cell. Summary of data obtained in a series of similar experiments shows that the rate of [Ca^{2+}]$_c$ rise and wave velocity were smaller in GFP-IP$_3$R$_{224-605}$-expressing cells than in non-transfected as well as in GFP-N-expressing cells (Fig. 5*, bar charts*; $p < 0.001$; $n = 6$). These results suggest that the regenerative mechanism of the [Ca^{2+}]$_c$ waves must involve an elevation of [IP$_3$] in COS-7 cells stimulated with IP$_3$-linked agonists. Previous work (44) has shown that varying concentrations of agonists elicit varying magnitudes of [^{3}H]IP$_3$ formation but induce [Ca^{2+}]$_c$ spikes that show a constant height and trigger [Ca^{2+}]$_c$ waves that exhibit a constant rate of progress in hepatocytes. When COS-7 cells were sequentially stimulated with a suboptimal (0.5 μM) and a maximally effective dose of ATP (200 μM), the lag time of the [Ca^{2+}]$_c$ wave was affected by the stimulus strength (6.3 ± 0.9 *versus* 3.0 ± 0.8 s, $p < 0.03$, $n = 5$), whereas the amplitude was stable ($\Delta F/F_0$, 0.58 ± 0.02 *versus* 0.56 ± 0.01, $n = 6$) similar to the results obtained in hepatocytes. However, the wave velocity was affected by the concentration of the agonist (32.3 ± 7.2 *versus* 55.8 ± 4.6 μm/s, $p < 0.02$, $n = 6$), indicating that in COS-7 cells the [Ca^{2+}]$_c$ wave velocity seems to be controlled by the agonist-induced IP$_3$ production. Thus, dampening of the cellular [IP$_3$] increase and modification of the timing of the rapid IP$_3$ diffusion may mediate the effect of GFP-IP$_3$R$_{224-605}$ on the regenerative mechanism of [Ca^{2+}]$_c$ wave propagation. Interestingly, a wave of IP$_3$ production has been recently claimed to underlie the fertilization Ca^{2+} wave in *Xenopus* oocytes (45). Because PIP$_2$ may exert an inhibition on the IP3R Ca^{2+} channel (46), cleavage of PIP$_2$ in the vicinity of the IP3Rs would not only provide IP$_3$ for channel activation but it could also relieve an inhibition elicited by PIP$_2$. The effect of IP3BPs may also involve attenuation of the effect of IP$_3$ formed close to the IP3Rs.

Effect of Cytosolic IP3BPs on Store-operated Ca^{2+} Entry—Comparison of the [Ca^{2+}]$_c$ signal of the GFP-IP$_3$R$_{224-605}$- or p130PH-GFP-expressing cells with that of cells expressing GFP alone showed that the IP3BP-dependent inhibition of the [Ca^{2+}]$_c$ signal was confined to the initial phase (2–5 min) of the stimulation by both ATP and EGF (Fig. 6, *A* and *B*). To separate Ca^{2+} entry from Ca^{2+} mobilization, the cells were placed next into a Ca^{2+}-free medium stimulated with ATP and Ca^{2+} was added back at 5 min of the stimulation (Fig. 6*C*). Also, the IP3BP was fused to monomeric RFP to minimize the bleed through to the fura2 fluorescence and Tg was added together with ATP to result in similar Ca^{2+} store depletion in each condition. The non-transfected and the RFP-alone transfected cells showed a robust ATP + Tg-induced [Ca^{2+}]$_c$ spike and, in response to the Ca^{2+} back addition, a rapid and massive elevation of [Ca^{2+}]$_c$ (Fig. 6*C*, *black* and *red traces*). The RFP-p130PH-expressing cells exhibited a slow and relatively small ATP + Tg-induced [Ca^{2+}]$_c$ spike, but the effect of the Ca^{2+} back addition was as prompt and large as it was in the non-trans-

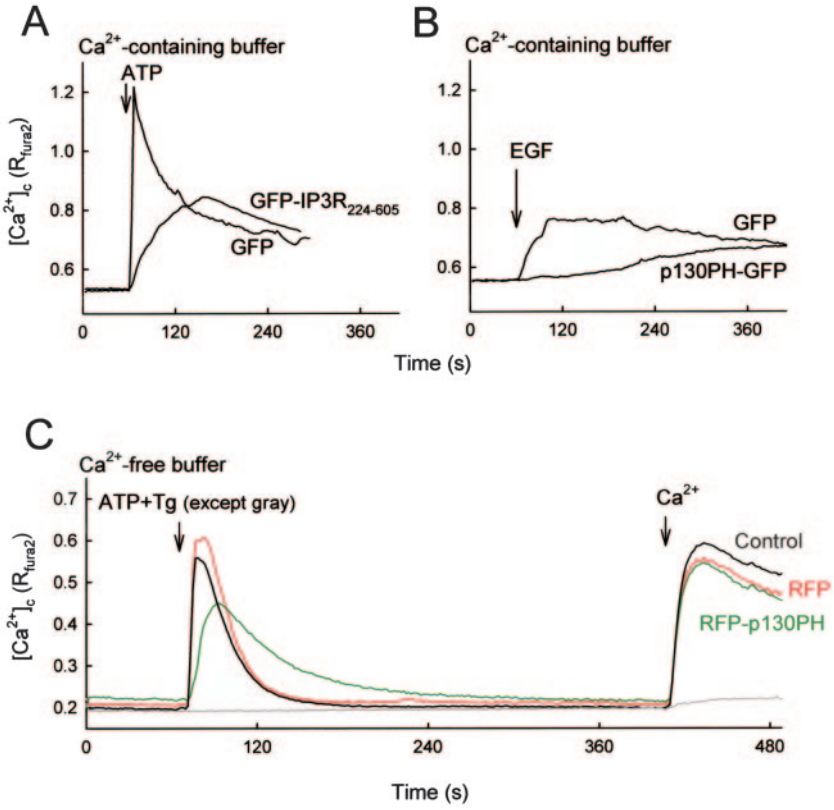

FIG. 6. **IP3BPs fail to affect the ATP-stimulated Ca^{2+} influx.** *A*, time course of the $[Ca^{2+}]_c$ signal induced by 50 μM ATP in GFP- and in GFP-IP$_3$R$_{224-605}$-expressing cells recorded with fura2. *Traces* show the mean response of the entire transfected cell population in the imaging field (8–15 cells) from 6–7 experiments. *B*, time course of the $[Ca^{2+}]_c$ signal induced by 100 ng/ml EGF in GFP- and in p130PH-GFP-expressing cells recorded with fura2. *Traces* represent the mean response of the entire transfected cell population in the imaging field (8–15 cells) from 6–7 experiments. *C*, ATP-stimulated Ca^{2+} entry in non-transfected cells (*black*), RFP-expressing cells (*red*), and RFP-p130PH-expressing cells (*green*). At a 5-min stimulation with 50 μM ATP and 2 μM Tg, Ca^{2+} influx was initiated by the addition of 2 mM $CaCl_2$. If Ca^{2+} was added back to non-stimulated cells, no substantial $[Ca^{2+}]_c$ signal was detected (*gray*). *Traces* represent the mean response calculated for the entire transfected and non-transfected cell population in the imaging field (6–10 transfected and 7–15 non-transfected cells, respectively) from four different experiments.

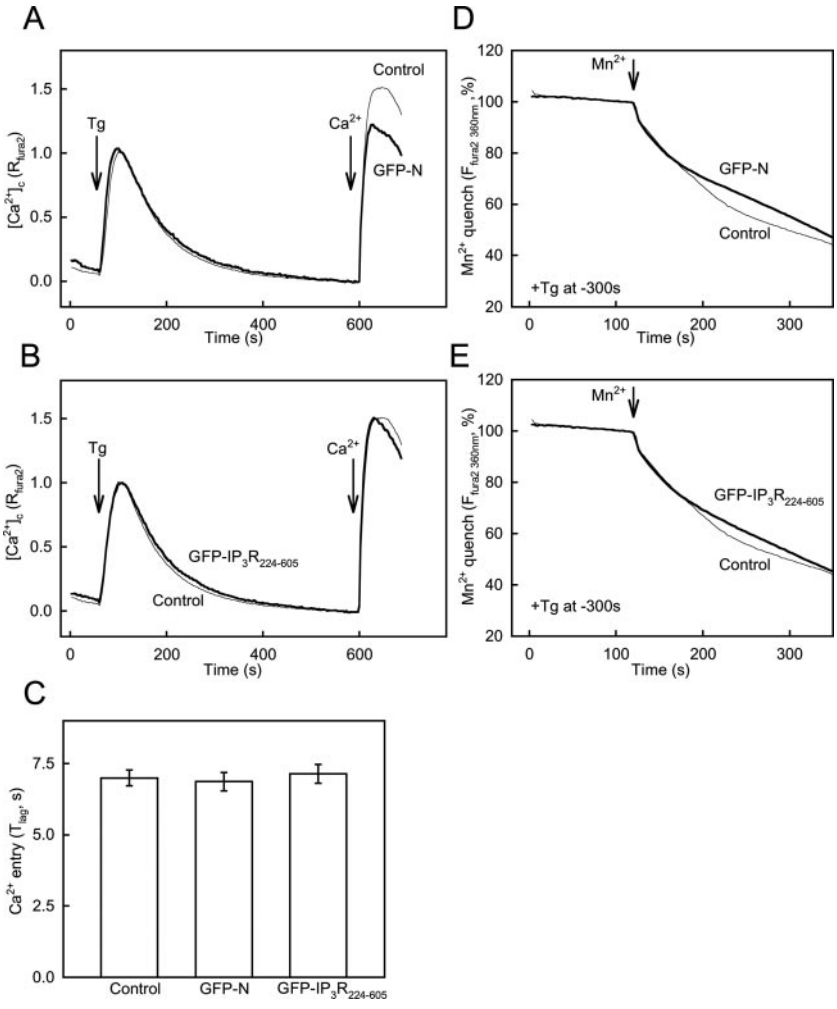

FIG. 7. **GFP-IP$_3$R$_{224-605}$ fails to affect Tg-induced Ca^{2+} entry in COS-7 cells.** *A* and *B*, measurement of Ca^{2+} entry. Cells transfected with GFP-N or GFP-IP$_3$R$_{224-605}$ were loaded with fura2 and were incubated in Ca^{2+}-free extracellular medium. Time course of $[Ca^{2+}]_c$ response elicited by sequential addition of 2 μM Tg and 1 mM $CaCl_2$ is shown. Change in the fluorescence ratio of fura2 (excited at 340/380 nm) was normalized to the maximal change evoked by Tg. *Traces* represent the mean response of control *versus* GFP-N and control *versus* GFP-IP$_3$R$_{224-605}$ cells. *C*, t_{lag} of Ca^{2+} entry in control, GFP-N, and GFP-IP$_3$R$_{224-605}$ cells. t_{lag} referred to the time needed to reach half of the maximal $[Ca^{2+}]_c$ rise. Data were the mean ± S.E. of values from the entire cell population in the imaging field (20–40 cells) from 4–5 different experiments. *D* and *E*, measurement of Mn^{2+} quench. Activation of the plasma membrane Ca^{2+} channel achieved by preincubating the cells with 2 μM Tg for 300 s was monitored by Mn^{2+}-induced (100 μM) quench of cytosolic fura2. The rate of quench reflected penetration of Mn^{2+} into the fura2-containing cytosol.

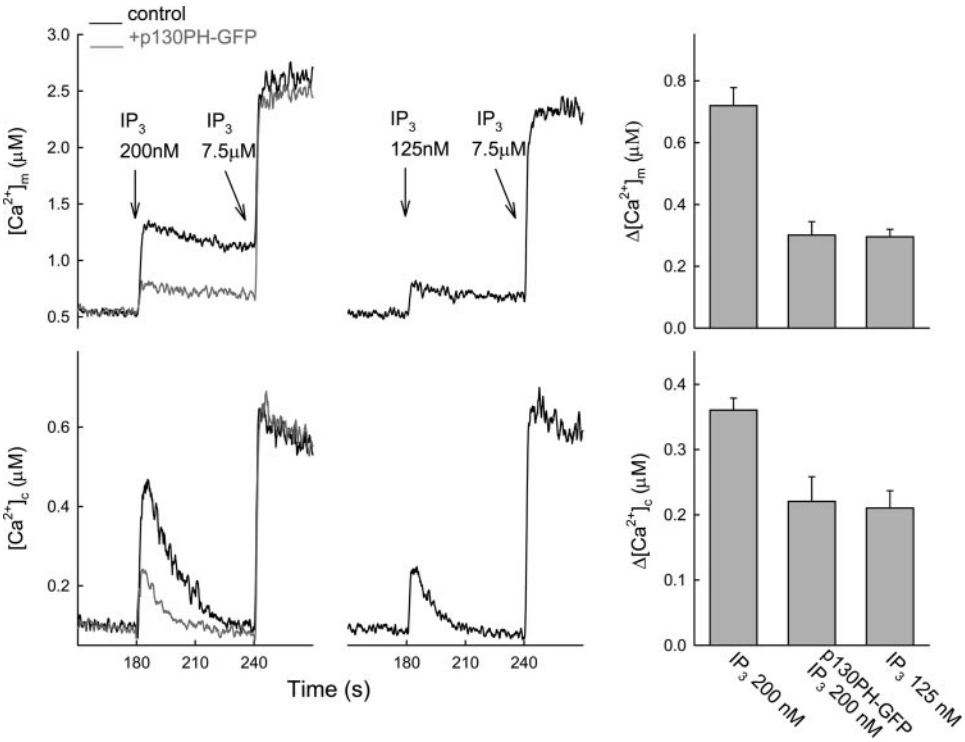

FIG. 8. **Inhibition by p130PH-GFP of the IP$_3$-induced [Ca^{2+}]$_m$ signal in permeabilized RBL-2H3 cells.** Simultaneous measurements of [Ca^{2+}]$_c$ and [Ca^{2+}]$_m$ responses were evoked by IP$_3$ in suspensions of fura2FF-loaded permeabilized RBL-2H3 cells. [Ca^{2+}]$_m$ was measured using compartmentalized fura2FF that has been shown to be confined to the mitochondria in this model (*upper*) (22), and [Ca^{2+}]$_c$ was followed with rhod2/FA (*lower*). IP$_3$-induced [Ca^{2+}]$_c$ and [Ca^{2+}]$_m$ responses were recorded in the presence (*gray*) or absence (*black*) of p130PH-GFP. *Right*, comparison of the magnitude of the [Ca^{2+}]$_c$ and [Ca^{2+}]$_m$ responses elicited by different [IP$_3$] in the presence or absence of p130PH-GFP (mean ± S.E., n = 4–5).

fected or RFP-expressing cells (Fig. 6*C*, *green trace*). Based on these results, the IP3BPs do not appear to affect the Ca^{2+} entry evoked by the IP_3-linked agonists.

Store-operated Ca^{2+} entry can be activated by ER Ca^{2+} depletion both in the presence and absence of a rise in total cellular [IP_3]. Recent studies have suggested that a portion of the IP_3-sensitive Ca^{2+} store is closely associated with the plasma membrane and interact with the store-operated Ca^{2+} channels in an IP_3-dependent manner to stimulate Ca^{2+} entry (conformational coupling, reviewed in Ref. 14). IP3BPs could have failed to inhibit the Ca^{2+} influx in the ATP-stimulated cells if the agonist-induced IP_3 signal was supramaximal for the Ca^{2+} entry. To determine whether any fluctuations in IP_3 are involved in the control of the coupling between Ca^{2+} release and entry, we investigated the Ca^{2+} entry in GFP-$IP_3R_{224-605}$-expressing cells using two fura2-imaging approaches. In the first protocol, cells were incubated in the absence of extracellular Ca^{2+}, the ER Ca^{2+} store was discharged using Tg, and then Ca^{2+} was added back to initiate Ca^{2+} entry (Fig. 7, *A* and *B*). The Tg-induced Ca^{2+} release appeared as a gradually rising and decaying [Ca^{2+}]$_c$ signal, whereas Ca^{2+} entry gave rise to a rapid and massive [Ca^{2+}]$_c$ signal (Fig. 7, *A* and *B*). The time course of the [Ca^{2+}]$_c$ signal resulting from intracellular Ca^{2+} mobilization and Ca^{2+} entry was not changed by the expression of GFP-N or GFP-$IP_3R_{224-605}$ in the cells (Fig. 7, *A* and *B*, *thick lines*). As a measure of the Ca^{2+} entry, we calculated the lag time of the Ca^{2+} addition-induced Ca^{2+} signal (Fig. 7*C*). There was no significant difference among control (6.99 ± 0.28 s), GFP-N (6.86 ± 0.32 s), and GFP-$IP_3R_{224-605}$ (7.13 ± 0.33 s). In the second approach, we used Mn^{2+} as a surrogate for Ca^{2+} to characterize unidirectional ion flux through store depletion-activated Ca^{2+} channels (Fig. 7, *D* and *E*). The rate of Mn^{2+} transport through this pathway was shown by the quench of fura2 fluorescence measured at 360 nm, a Ca^{2+}-independent excitation wavelength. Specifically, cells were pretreated with Tg for 300 s to deplete the ER Ca^{2+} store and to activate Ca^{2+} entry and then $MnCl_2$ was added (Fig. 7, *D* and *E*). The time course of Mn^{2+} quench was not affected by the presence of GFP-$IP_3R_{224-605}$ (Fig. 7, *E versus* D). These results show that buffering of IP_3 does not interfere with the activation of Ca^{2+} entry during depletion of the ER Ca^{2+} store. Notably, we tested Ca^{2+} entry only after complete store depletion had been reached; therefore, the results do not exclude the possibility that the kinetic of the activation of Ca^{2+}entry is modulated by IP_3 (reviewed in Ref. 47).

Effect of Cytosolic IP3BPs on the Propagation of [Ca^{2+}]$_c$ Signals into the Mitochondria—In a wide variety of cell types, the IP_3-induced Ca^{2+} mobilization is effectively propagated to the mitochondria (for a summary see Table I in Ref. 48). Mitochondria form local interactions with subdomains of the ER (24), and at the sites of interaction, mitochondrial Ca^{2+} uptake is tightly coupled to IP3R-mediated Ca^{2+} release reminiscent of the organization of synaptic transmission (22). However, the functional organization of the local communication remains elusive. Using the IP3BPs, we tested the IP_3 requirements for the ER-mitochondrial Ca^{2+} coupling. We first used a permeabilized cell model that allowed fluorometric measurement of [Ca^{2+}]$_m$ simultaneously with [Ca^{2+}]$_c$ during IP_3-induced Ca^{2+} mobilization (22, 49). As we noted for the [Ca^{2+}]$_c$ signal (Fig. 2), the [Ca^{2+}]$_m$ elevations evoked by the addition of a submaximal IP_3 were also suppressed in the presence of p130PH-GFP (125 nM) (Fig. 8, *upper left*). Importantly, the suppression of the [Ca^{2+}]$_m$ signal was large compared with the attenuation of the [Ca^{2+}]$_c$ signal (mean ± S.D. responses are shown in the *bar charts*). We have shown earlier that the IP_3 dose response for [Ca^{2+}]$_m$ rise is shifted rightward compared with the IP_3 dose response for Ca^{2+} release (22). We speculated that the difference between [Ca^{2+}]$_c$ and [Ca^{2+}]$_m$ dose response relations may

contribute to the relatively large inhibition of the IP_3-induced $[Ca^{2+}]_m$ rise by p130PH-GFP. By lowering the dose of IP_3, we found that 125 nM IP_3 evoked a $[Ca^{2+}]_c$ signal identical to that of 200 nM IP_3 in the presence of 125 nM p130PH-GFP (Fig. 8). Furthermore, 125 nM IP_3 elicited a $[Ca^{2+}]_m$ rise that was comparable to the effect of 200 nM IP_3 in the presence of 125 nM p130PH-GFP (Fig. 8). Based on these data, IP3BPs suppress the Ca^{2+} release mediated by the IP3Rs that provide Ca^{2+} for mitochondrial Ca^{2+} uptake. Furthermore, suppression of Ca^{2+} release results in attenuation of the $[Ca^{2+}]_m$ signal more than the $[Ca^{2+}]_c$ rise. An important clue to this point is that a second-order relationship exists between $[Ca^{2+}]_c$ and the mitochondrial Ca^{2+} uptake (for review see Ref. 50).

To evaluate in intact cells the calcium signal propagation to the mitochondria, we carried out measurements of $[Ca^{2+}]_m$ with ratiometric pericam-mt (37). Because the fluorescence spectrum of pericam-mt is similar to the spectrum of enhanced GFP, p130PH was introduced to the cells fused to RFP. Simultaneous recording of F_{RFP}, $F_{pericam\text{-}mt}$, and F_{fura2} was achieved by combination of a filter wheel with a motorized turret, which permitted the selection of the appropriate excitation filters and filter cubes containing the dichroic reflectors and emission filters. Although this design allowed us to minimize the cross-talk between fluorophores, $F_{pericam\text{-}mt}$ was still detectable at 380-nm excitation, one of the excitation wavelengths used for fura2. Because pericam-mt was always excluded from the nucleus, the nuclear area was selected in each cell to calculate $[Ca^{2+}]_c$. As shown in Fig. 9, most of the cells expressing either RFP-N or RFP-p130PH also expressed pericam-mt (*upper two rows* of *images*) and the subcellular distribution of pericam-mt was similar to the distribution of enhanced GFP targeted to the mitochondria (Fig. 1*B*, *iv*). Furthermore, during stimulation with ATP, the cells expressing RFP alone displayed a substantial change in pericam-mt fluorescence, and the change in fluorescence followed distribution of the mitochondria. In contrast, the RFP-p130PH-expressing cells showed little or no change in pericam-mt fluorescence (Fig. 8, *third row* of *images*). To quantitate $[Ca^{2+}]_c$ and $[Ca^{2+}]_m$, for every cell, the fura2 and pericam ratios were obtained and then the cell population average was calculated (Fig. 9, *graphs*). In RFP-N cells, the ATP-induced $[Ca^{2+}]_c$ rise (*left panel*, *blue trace*) was followed by a large $[Ca^{2+}]_m$ transient with a hardly noticeable delay (*left panel*, *red trace*). In the RFP-p130PH-expressing cells, the onset of the $[Ca^{2+}]_c$ rise was somewhat delayed and the peak was smaller (*right panel*, *blue trace*) but the $[Ca^{2+}]_m$ signal was almost abolished (*right panel*, *red trace*). Similar observations were made when GFP-$IP_3R_{224-605}$ was expressed in the cells and $[Ca^{2+}]_m$ was monitored with rhod2 compartmentalized to the mitochondria ($n = 3$, data not shown). Thus, in intact cells, despite the small decrease in the $[Ca^{2+}]_c$ signal, the suppression of the $[Ca^{2+}]_m$ signal by the IP3BPs was almost complete. Because individual mitochondria appear to utilize discrete paths of local communication to access the Ca^{2+} released from the ER, subpopulations of mitochondria could be less sensitive to the increase in IP_3-buffering capacity than others. We acquired images at higher spatial resolution to evaluate the ATP-induced $[Ca^{2+}]_m$ signal in several small groups of mitochondria in individual RFP-p130PH-expressing cells (Fig. 10). The large $[Ca^{2+}]_c$ spike was not associated with a considerable $[Ca^{2+}]_m$ increase in any of the mitochondria (Fig. 10, *red traces*).

To further investigate the relationship between the agonist-induced Ca^{2+} mobilization and the $[Ca^{2+}]_m$ signal, the $[Ca^{2+}]_c$ and $[Ca^{2+}]_m$ rise was calculated for the individual cells expressing either RFP or RFP-p130PH and the $[Ca^{2+}]_m$ was plotted over a range of $[Ca^{2+}]_c$ values attained in different single cells (Fig. 11). The distribution of the points representing

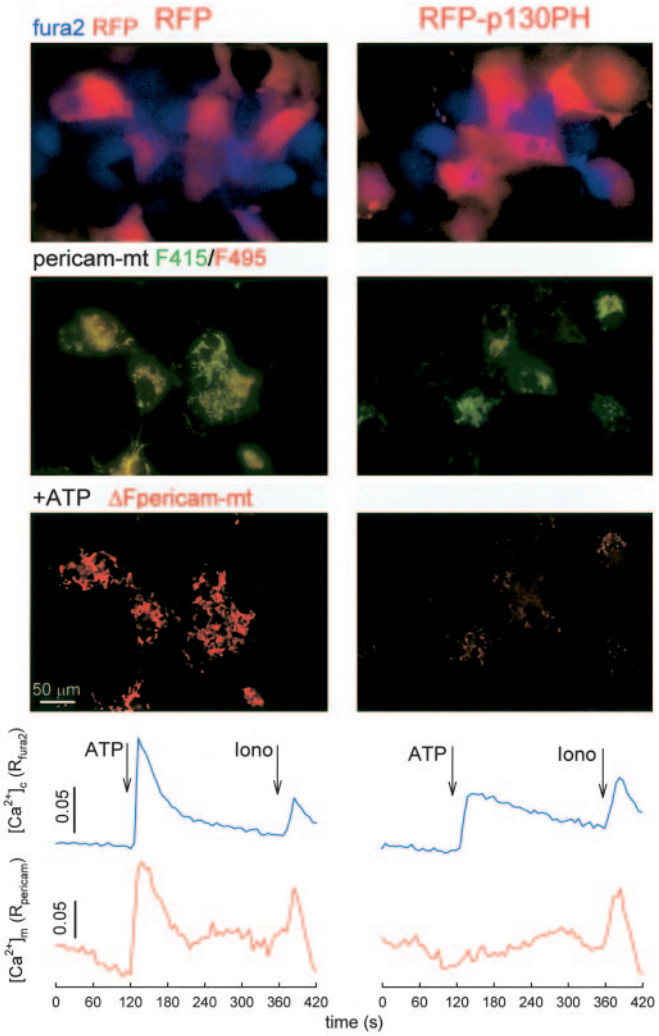

FIG. 9. **Effect of RFP-p130PH on the $[Ca^{2+}]_m$ signal in intact COS-7 cells.** Fluorescence imaging of RFP and pericam-mt was carried out simultaneously with imaging of fura2 in cells transfected with either RFP or RFP-p130PH. fura2 (340-nm excitation) and RFP fluorescence are shown as *blue/red overlays* (*upper*), pericam-mt fluorescence is shown as *green/red overlay* of the images obtained at 414- and 495-nm excitations (*middle*), and the spatial distribution of 50 μM ATP-induced change in pericam-mt fluorescence is shown as a difference calculated for the images obtained before and after stimulation with ATP (50 μM) (*lower*). Mean fura2 and pericam-mt ratios calculated for all of the cells expressing both RFP and pericam obtained from four measurements of each condition are shown in the *graphs*. *Iono*, ionomycin.

the RFP-p130PH cells suggests that these cells show a relatively small $[Ca^{2+}]_m$ rise at any given $[Ca^{2+}]_c$ signal (Fig. 11, *upper panel*). As an example, the mean $[Ca^{2+}]_c$ and $[Ca^{2+}]_m$ responses were calculated for the RFP and RFP-p130PH cells that displayed 50–150% increase in the fura2 ratio. The mean $[Ca^{2+}]_c$ signal was similar in both the control and the IP_3 buffer-expressing cells, but the $[Ca^{2+}]_m$ rise was reduced by >80% in the RFP-p130PH cells (Fig. 11, *lower panel*). Thus, the $[Ca^{2+}]_m$ *versus* $[Ca^{2+}]_c$ relationship is altered in the presence of the IP3BPs.

Collectively, these data showed that the IP_3-induced $[Ca^{2+}]_m$ signal in the permeabilized cells and the agonist-induced $[Ca^{2+}]_m$ signal in the intact cells are largely suppressed in the presence of IP3BPs. Both in permeabilized and in intact cells, the $[Ca^{2+}]_m$ is more sensitive to the IP3BPs than the global $[Ca^{2+}]_c$ signal that can be considered as a measure of the amount of mobilized Ca^{2+}. The high sensitivity of the $[Ca^{2+}]_m$ signal to the IP3BPs can be attributed to a non-linear relation-

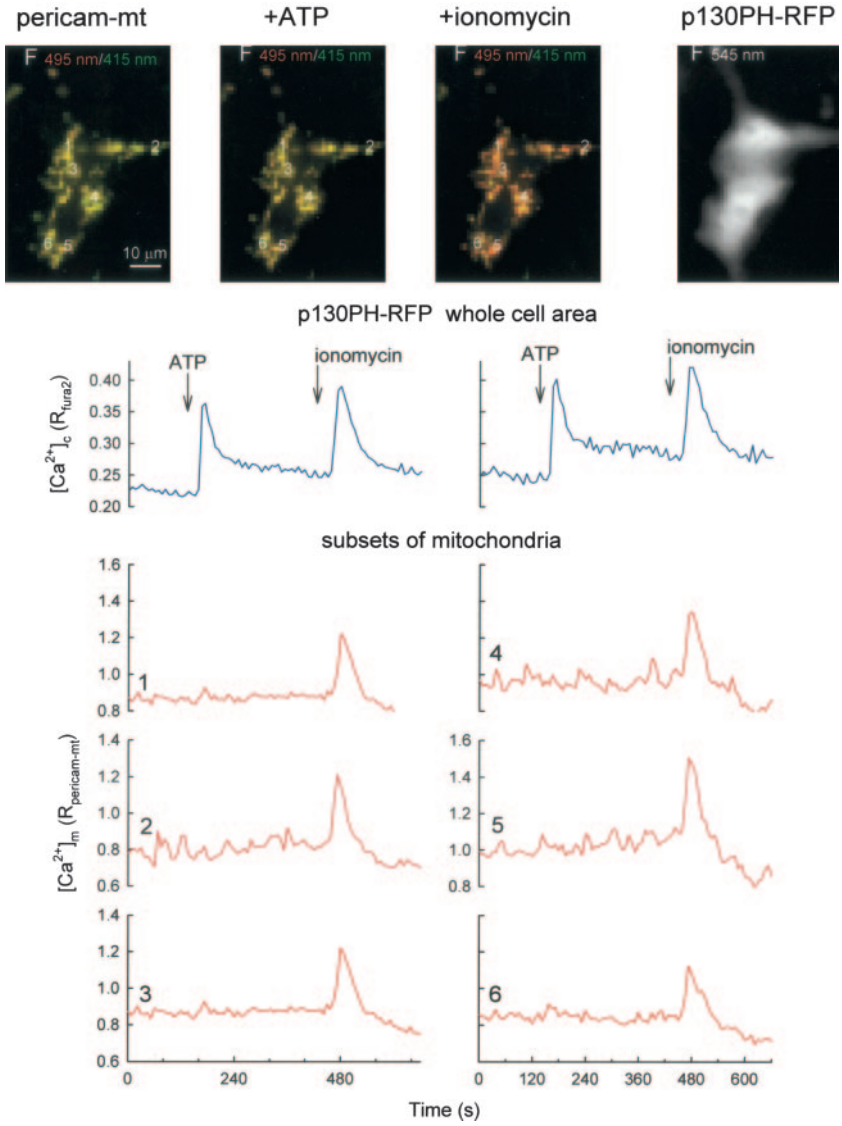

FIG. 10. **[Ca^{2+}]$_m$ in subsets of mitochondria in cells expressing RFP-p130PH.** Fluorescence imaging of RFP and ratiometric pericam-mt was carried out simultaneously with the imaging of fura2 in cells transfected with RFP-p130PH. RFP fluorescence is shown (*grayscale*; *right*) to mark the position and shape of the two cells on the field. Pericam-mt fluorescence (*green/red overlay*) is shown before stimulation, after the addition of ATP (50 μM), and after the addition of ionomycin (10 μM). Time courses of [Ca^{2+}]$_c$ for each whole cell (*blue*) and [Ca^{2+}]$_m$ for the numbered subsets of mitochondria (2.4 × 2.4 μm; *red*) are shown. The data are representative of experiments repeated six times.

ship between [Ca^{2+}]$_c$ and mitochondrial Ca^{2+} uptake/[Ca^{2+}]$_m$, which has been documented for both isolated mitochondria (for review see Ref. 50) and permeabilized cells (22, 23). The Ca^{2+} dependence of the [Ca^{2+}]$_m$ is apparently unaffected by IP3BPs in the permeabilized cells, because in this model, both the [Ca^{2+}]$_c$ and [Ca^{2+}]$_m$ signals evoked by a given dose of IP$_3$ in the presence of an IP3BP could be reproduced by the addition of a lower dose of IP$_3$ alone (Fig. 8). However, in the intact cells, the mitochondria were effectively dissociated from the global [Ca^{2+}]$_c$ signal by the IP3BPs (Figs. 9 and 10) and depression of the [Ca^{2+}]$_c$ dependence of the [Ca^{2+}]$_m$ signal was also shown (Fig. 11). The key to this point seems to be that the Ca^{2+} uptake of the mitochondria depends on a local perimitochondrial [Ca^{2+}]$_c$ rise mediated by the adjacent IP3Rs (21, 22, 24). We have shown that activation of a cluster of Ca^{2+} release sites is sufficient to evoke a [Ca^{2+}]$_m$ signal ("Ca^{2+} mark") (26) but that optimal activation of the mitochondrial Ca^{2+} uptake sites requires coordinated activation of the IP3Rs that deliver Ca^{2+} to the mitochondria (22). Such coordinated activation of the IP3Rs is expected to be largely affected in the presence of an IP$_3$ buffer, resulting in suppression of the local [Ca^{2+}]$_c$ signal even if the total Ca^{2+} release and the cellular average [Ca^{2+}]$_c$ signal show little or no attenuation. Thus, the relationship between the global [Ca^{2+}]$_c$ and [Ca^{2+}]$_m$ may show a change in the presence of the IP3BPs in intact cells because the relationship between the local, perimitochondrial [Ca^{2+}]$_c$, and the global [Ca^{2+}]$_c$ is altered. We reason that the [Ca^{2+}]$_m$ signal was more sensitive to IP3BPs in intact cells than in permeabilized cells, because IP$_3$ was added as a bolus to the permeabilized cells, whereas it was produced by PLCs in intact cells, enabling the IP3BPs to decrease the rate of [IP$_3$] rise.

CONCLUSIONS

The most important observation of this study is that the propagation of the [Ca^{2+}]$_c$ signal to the mitochondria is strikingly sensitive to the IP$_3$-buffering power of the cytoplasm. Thus, the kinetics and spatial distribution of the [IP$_3$] rise appear to control the recruitment of the mitochondrial Ca^{2+} buffering and ATP production to the [Ca^{2+}]$_c$ signal. Our work also evaluated for, the first time, the effect of IP$_3$ buffers on Ca^{2+} wave propagation and on store-operated Ca^{2+} entry and has provided evidence that the rapid increase in [IP$_3$] is important for the regenerative mechanism of the [Ca^{2+}]$_c$ wave but that rapid fluctuations in [IP$_3$] may not be required for the optimal activation of Ca^{2+} entry by store depletion.

The IP$_3$ signal has been envisioned to originate from the G$_q$- or tyrosine kinase-stimulated activation of PLC and hydrolysis of PIP$_2$ at the plasma membrane and to utilize rapid diffusion of IP$_3$ throughout the cells. However, recent studies have indicated that Ca^{2+}-induced IP$_3$ formation may also occur at intra-

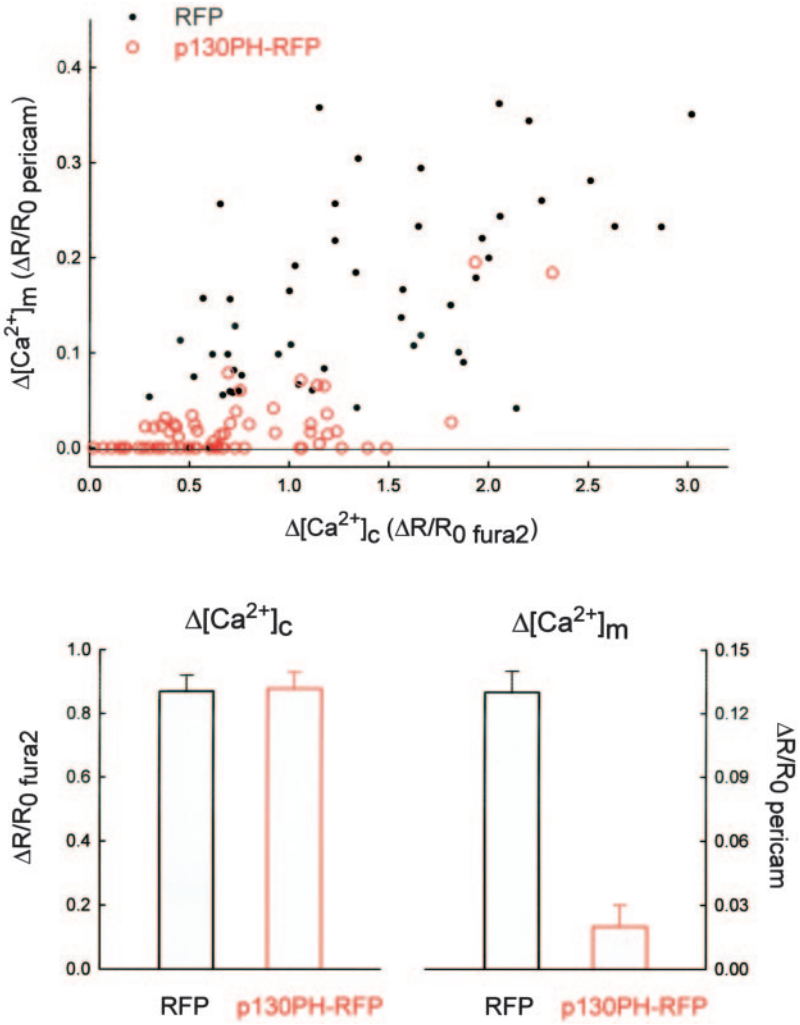

FIG. 11. **RFP-p130PH decreases the relationship between $[Ca^{2+}]_c$ and $[Ca^{2+}]_m$ during the IP_3-linked calcium signal.** In the experiments shown in Figs. 8 and 9, the $[Ca^{2+}]_c$ and $[Ca^{2+}]_m$ rise was calculated for the individual cells and the $[Ca^{2+}]_m$ was plotted over a range of $[Ca^{2+}]_c$ values attained in different single cells in the presence of RFP or RFP-p130PH (*upper panel*). For both the RFP and RFP-p130PH cells that showed 50–150% increase in the fura2 ratio, the average $[Ca^{2+}]_c$ and $[Ca^{2+}]_m$ responses were plotted (*lower panel*).

cellular membranes (9–11). Furthermore, IP_3-binding proteins are expressed in several cell types and may also contribute to the shaping of the $[IP_3]$ signal (*e.g.* p130) (29–33). Thus, the $[IP_3]$ signal may display a complex spatio-temporal pattern. Overexpression of IP_3-binding proteins provided us with a tool to change the temporal pattern of the $[IP_3]$ rise and to interfere with spatially confined fluctuations in $[IP_3]$. Our data indicate that the kinetics of the $[IP_3]$ signal affects both the initiation and the propagation of the $[Ca^{2+}]_c$ signal. Along this line, regional differences in IP_3 production and buffering may converge with regional differences in the Ca^{2+} feedback on the IP3R/RyR to generate regional differences in $[Ca^{2+}]_c$ wave velocity, which have been observed in several models. If an increase in IP_3 buffering leads to slower propagation of the $[Ca^{2+}]_c$ wave but at each location the size of the $[Ca^{2+}]_c$ rise is relatively stable, the activation of cytoplasmic Ca^{2+} effectors may remain unaffected. Also, IP_3 buffers fail to modulate the store depletion-induced Ca^{2+} entry, providing evidence that neither a global nor a local increase in IP_3 production is involved in the coupling between massive ER Ca^{2+} depletion and store-operated Ca^{2+} entry. By contrast, the presence of IP_3 buffers results in a dramatic inhibition of mitochondrial Ca^{2+} accumulation during the agonist-induced $[Ca^{2+}]_c$ signal. The large effect of the IP_3 buffer on mitochondrial Ca^{2+} uptake could be partly explained by its non-linear dependence on extramitochondrial $[Ca^{2+}]$. However, we demonstrate that the relationship between the $[Ca^{2+}]_c$ and $[Ca^{2+}]_m$ signals is also suppressed when the IP_3 buffering is enhanced. A clue to this problem is that coordinated activation of the IP3Rs seems to be important for mitochondrial Ca^{2+} uptake (22) and that IP_3 buffers may influence the rate of global $[IP_3]$ increase or attenuate a local $[IP_3]$ signal to compromise synchronized opening of the IP3Rs.

Taken together, the present results show IP3BPs as a valuable tool in the study of the mechanisms of local calcium signaling and indicate that a dynamic local interplay between Ca^{2+} and IP_3 is of great significance for the propagation of the calcium signal throughout the cytosol and into the mitochondria. Furthermore, based on their relatively large effect on the $[Ca^{2+}]_m$ signal, IP3BPs may provide a tool to selectively attenuate the mitochondrial effects of the $[Ca^{2+}]_c$ signal and can be useful to determine the mitochondrial contribution in a range of signaling cascades.

Acknowledgments—We thank David Weaver for help with confocal imaging. We are grateful to Dr. Roger Y. Tsien for the monomeric red fluorescent protein.

REFERENCES

1. Berridge, M. J., Bootman, M. D., and Roderick, H. L. (2003) *Nat. Rev. Mol. Cell. Biol.* **4,** 517–529
2. Wakui, M., Potter, B. V., and Petersen, O. H. (1989) *Nature* **339,** 317–320
3. Lechleiter, J. D., and Clapham, D. E. (1992) *Cell* **69,** 283–294
4. Callamaras, N., Marchant, J. S., Sun, X. P., and Parker, I. (1998) *J. Physiol. (Lond.)* **509,** 81–91
5. Rooney, T. A., Renard, D. C., Sass, E. J., and Thomas, A. P. (1991) *J. Biol. Chem.* **266,** 12272–12282
6. Harootunian, A. T., Kao, J. P., Paranjape, S., and Tsien, R. Y. (1991) *Science* **251,** 75–78
7. Young, K. W., Nash, M. S., Challiss, R. A., and Nahorski, S. R. (2003) *J. Biol. Chem.* **278,** 20753–20760
8. Meyer, T., and Stryer, L. (1991) *Annu. Rev. Biophys. Biophys. Chem.* **20,** 153–174

9. Rice, A., Parrington, J., Jones, K. T., and Swann, K. (2000) *Dev. Biol.* **228,** 125–135
10. Lee, S. B., Varnai, P., Balla, A., Jalink, K., Rhee, S. G., and Balla, T. (2004) *J. Biol. Chem.* **279,** 24362–24371
11. Watt, S. A., Kular, G., Fleming, I. N., Downes, C. P., and Lucocq, J. M. (2002) *Biochem. J.* **363,** 657–666
12. Allbritton, N. L., Meyer, T., and Stryer, L. (1992) *Science* **258,** 1812–1815
13. Putney, J. W., Jr. (2004) *Trends Cell Biol.* **14,** 282–286
14. Putney, J. W., Jr., Broad, L. M., Braun, F. J., Lievremont, J. P., and Bird, G. S. (2001) *J. Cell Sci.* **114,** 2223–2229
15. Parekh, A. B. (2003) *J. Physiol.* (*Lond.*) **547,** 333–348
16. Takemura, H., Hughes, A. R., Thastrup, O., and Putney, J. W., Jr. (1989) *J. Biol. Chem.* **264,** 12266–12271
17. Kiselyov, K., Mignery, G. A., Zhu, M. X., and Muallem, S. (1999) *Mol. Cell* **4,** 423–429
18. Ma, H. T., Venkatachalam, K., Rys-Sikora, K. E., He, L. P., Zheng, F., and Gill, D. L. (2003) *Biochem. J.* **376,** 667–676
19. Jouaville, L. S., Pinton, P., Bastianutto, C., Rutter, G. A., and Rizzuto, R. (1999) *Proc. Natl. Acad. Sci. U. S. A.* **96,** 13807–13812
20. Hajnoczky, G., Robb-Gaspers, L. D., Seitz, M. B., and Thomas, A. P. (1995) *Cell* **82,** 415–424
21. Rizzuto, R., Brini, M., Murgia, M., and Pozzan, T. (1993) *Science* **262,** 744–747
22. Csordas, G., Thomas, A. P., and Hajnoczky, G. (1999) *EMBO J.* **18,** 96–108
23. Szalai, G., Csordas, G., Hantash, B. M., Thomas, A. P., and Hajnoczky, G. (2000) *J. Biol. Chem.* **275,** 15305–15313
24. Rizzuto, R., Pinton, P., Carrington, W., Fay, F. S., Fogarty, K. E., Lifshitz, L. M., Tuft, R. A., and Pozzan, T. (1998) *Science* **280,** 1763–1766
25. Sparagna, G. C., Gunter, K. K., Sheu, S. S., and Gunter, T. E. (1995) *J. Biol. Chem.* **270,** 27510–27515
26. Pacher, P., Thomas, A. P., and Hajnoczky, G. (2002) *Proc. Natl. Acad. Sci. U. S. A.* **99,** 2380–2385
27. Rizzuto, R., Duchen, M. R., and Pozzan, T. (2004) *Science's STKE* http://stke.sciencemag.org/cgi/content/full/sigtrans;2004/53/re1
28. Hajnoczky, G., Csordas, G., Madesh, M., and Pacher, P. (2000) *J. Physiol.* (*Lond.*) **529,** 69–81
29. Maeda, N., Niinobe, M., and Mikoshiba, K. (1990) *EMBO J.* **9,** 61–67
30. Yoshikawa, F., Iwasaki, H., Michikawa, T., Furuichi, T., and Mikoshiba, K. (1999) *J. Biol. Chem.* **274,** 316–327
31. Varnai, P., Lin, X., Lee, S. B., Tuymetova, G., Bondeva, T., Spat, A., Rhee, S. G., Hajnoczky, G., and Balla, T. (2002) *J. Biol. Chem.* **277,** 27412–27422
32. Uchiyama, T., Yoshikawa, F., Hishida, A., Furuichi, T., and Mikoshiba, K. (2002) *J. Biol. Chem.* **277,** 8106–8113
33. Kanematsu, T., Takeya, H., Watanabe, Y., Ozaki, S., Yoshida, M., Koga, T., Iwanaga, S., and Hirata, M. (1992) *J. Biol. Chem.* **267,** 6518–6525
34. Kanematsu, T., Jang, I. S., Yamaguchi, T., Nagahama, H., Yoshimura, K., Hidaka, K., Matsuda, M., Takeuchi, H., Misumi, Y., Nakayama, K., Yamamoto, T., Akaike, N., and Hirata, M. (2002) *EMBO J.* **21,** 1004–1011
35. Takeuchi, H., Oike, M., Paterson, H. F., Allen, V., Kanematsu, T., Ito, Y., Erneux, C., Katan, M., and Hirata, M. (2000) *Biochem. J.* **349,** 357–368
36. Campbell, R. E., Tour, O., Palmer, A. E., Steinbach, P. A., Baird, G. S., Zacharias, D. A., and Tsien, R. Y. (2002) *Proc. Natl. Acad. Sci. U. S. A.* **99,** 7877–7882
37. Nagai, T., Sawano, A., Park, E. S., and Miyawaki, A. (2001) *Proc. Natl. Acad. Sci. U. S. A.* **98,** 3197–3202
38. Nakanishi, S., Catt, K. J., and Balla, T. (1995) *Proc. Natl. Acad. Sci. U. S. A.* **92,** 5317–5321
39. Pacher, P., and Hajnoczky, G. (2001) *EMBO J.* **20,** 4107–4121
40. Bolsover, S., Ibrahim, O., O'Luanaigh, N., Williams, H., and Cockcroft, S. (2001) *Biochem. J.* **356,** 345–352
41. Csordas, G., and Hajnoczky, G. (2001) *Cell Calcium* **29,** 249–262
42. Verkman, A. S. (2002) *Trends Biochem. Sci.* **27,** 27–33
43. van der Wal, J., Habets, R., Varnai, P., Balla, T., and Jalink, K. (2001) *J. Biol. Chem.* **276,** 15337–15344
44. Rooney, T. A., Sass, E. J., and Thomas, A. P. (1990) *J. Biol. Chem.* **265,** 10792–10796
45. Wagner, J., Fall, C. P., Hong, F., Sims, C. E., Allbritton, N. L., Fontanilla, R. A., Moraru, I. I., Loew, L. M., and Nuccitelli, R. (2004) *Cell Calcium* **35,** 433–447
46. Lupu, V. D., Kaznacheyeva, E., Krishna, U. M., Falck, J. R., and Bezprozvanny, I. (1998) *J. Biol. Chem.* **273,** 14067–14070
47. Venkatachalam, K., van Rossum, D. B., Patterson, R. L., Ma, H. T., and Gill, D. L. (2002) *Nat. Cell Biol.* **4,** E263–272
48. Hajnoczky, G., Csordas, G., and Yi, M. (2002) *Cell Calcium* **32,** 363–377
49. Csordas, G., Madesh, M., Antonsson, B., and Hajnoczky, G. (2002) *EMBO J.* **21,** 2198–2206
50. Gunter, T. E., and Pfeiffer, D. R. (1990) *Am. J. Physiol.* **258,** C755–C786